photonics

MDPI

Review

Two-Photon Microscopy in Biological Imaging: Current Uses and Evolving Potential

Qingpan Bu [1], Yinghui Gu [1], Xiaodan Wang [1], Shiwei Yuan [1], Kai Song [1,*] and Xingyun Zhang [2,*]

[1] School of Life Sciences, Changchun Normal University, Changchun 130032, China; buqingpan@ccsfu.edu.cn (Q.B.); qx202510003@stu.ccsfu.edu.cn (Y.G.); qx202510031@stu.ccsfu.edu.cn (X.W.); qx202510002@stu.ccsfu.edu.cn (S.Y.)

[2] Changchun Institute of Optics, Fine Mechanics and Physics, Chinese Academy of Sciences, Changchun 130033, China

* Correspondence: songkai@ccsfu.edu.cn (K.S.); xyzhang@ciomp.ac.cn (X.Z.)

Abstract

Two-photon microscopy (TPM) has become an indispensable tool in the life sciences, offering exceptional spatial resolution, deep tissue penetration, and low phototoxicity. It provides a revolutionary solution for long-term dynamic observation of living cells and tissues. This article systematically explains the working principles of TPM and reviews its applications in cutting-edge fields such as neuroscience, immunology, oncology, regenerative science and plant biology, highlighting its remarkable multidisciplinary adaptability. Building on this foundation, we further explore the breakthrough directions and future prospects for the development of this technology.

Keywords: two-photon microscopy; life sciences; living imaging; evolving potential

1. Introduction

Two-photon absorption refers to the quantum process in which molecules or atoms simultaneously absorb two photons under high photon density conditions, subsequently transitioning to an excited state. This theory was first proposed by Nobel laureate Goeppert-Mayer M. in 1931 [1]. However, due to limitations in light source technology at the time, the phenomenon remained experimentally unverified for decades. It was not until the 1960s, when laser technology achieved breakthroughs, that two-photon excitation and absorption effects were experimentally confirmed [2]. In 1990, the research team led by Denk W. at Cornell University innovatively combined two-photon absorption principles with laser scanning technology, successfully developing the world's first two-photon microscopy (TPM) [3].

Compared to traditional confocal laser scanning microscopes, TPM has rapidly become an indispensable tool in biological research due to its unique advantages: Firstly, near-infrared excitation light significantly reduces phototoxicity, enabling long-term imaging of live cells. Secondly, its exceptional tissue penetration capability allows for high-resolution imaging of thick samples. Thirdly, its intrinsic three-dimensional (3D) imaging capability provides a new perspective for in vivo studies [4–6]. This non-invasive imaging technology not only maximally preserves the physiological activity of biological samples, but also captures life dynamics within tissues that are difficult to observe with conventional methods.

In cutting-edge fields such as live cell dynamic monitoring, neural network activity tracking, and drug action mechanism research, this technology demonstrates irreplaceable advantages. It enables scientists to observe complex biological processes in real-time,

Check for updates

Received: 16 April 2026
Revised: 18 May 2026
Accepted: 20 May 2026
Published: 27 May 2026

Copyright: © 2026 by the authors. Licensee MDPI, Basel, Switzerland. This article is an open access article distributed under the terms and conditions of the Creative Commons Attribution (CC BY) license.

including cellular interactions, neural signal transmission, and immune responses, providing unprecedented research tools for unraveling the essence of life. Currently, this technology has been widely applied in disciplines such as cell biology, neuroscience, and immunology, not only driving breakthroughs in fundamental research but also serving as a crucial support for technological innovation in fields like biomedical engineering and drug development.

This article aims to provide a detailed introduction to the technical principles, key components, and distinctive features of TPM, as well as its integration with other technologies. It systematically reviews the diverse applications of TPM in biological imaging, which are categorized into distinct sections covering neuroscience, immunology, oncology, regenerative science and plant biology. Finally, this review discusses the current technical challenges and future development trends of TPM, aiming to establish a comprehensive reference framework for researchers in related fields.

2. Excitation Principle and Characteristics of Two-Photon Microscope

TPM is a fluorescence imaging technique that integrates confocal laser scanning microscopy with two-photon excitation technology, as illustrated in Figure 1. The system mainly consists of a femtosecond laser, an electro-optical modulator (EOM) or acousto-optic modulator (AOM), a scanning galvanometer (SG), a scan lens, a tube lens, an objective, a dichroic mirror (DM), a photodetector (PMT), a control computer and host software. The femtosecond laser in the near-infrared band serves as the key light source for achieving two-photon excitation. The SG employs two mutually perpendicular galvanometers (in the X and Y directions) to perform two-dimensional (2D) scanning of the laser beam across the sample. The DM separates the excitation and emission light paths by reflecting the near-infrared excitation light while transmitting the fluorescence signals in the visible range to the PMT. The PMT captures weak fluorescence signals and converts them into electrical signals for image reconstruction. The computer controls the scanning trajectory, acquires signals, reconstructs images, and performs 3D visualization and quantitative analysis. Although not strictly essential, the EOM (or AOM) is a key component of high-performance TPM systems, enabling precise and high-speed laser power control. For example, when imaging at varying tissue depths or using multiple fluorescent probes, the EOM (or AOM) can dynamically adjust the laser power to balance signal intensity, thereby enhancing image uniformity and contrast.

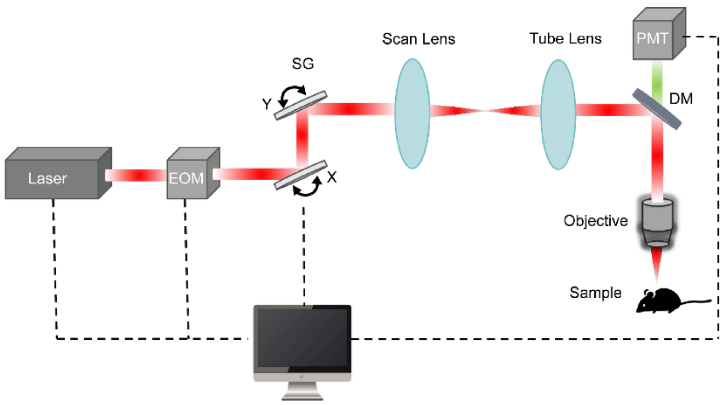

Figure 1. Typical schematic diagram of TPM.

The wavelength of the laser used in TPM typically falls within the near-infrared range of 680–1300 nm, with 700–1000 nm being the most commonly adopted interval; this spectral band boasts strong penetration capability, minimal scattering and absorption in biological tissues, enabling deep imaging ranging from hundreds of micrometers to millimeters. Opti-

mal wavelength selection is primarily contingent upon the two-photon fluorescence brightness spectrum of the target fluorophore—a composite metric integrating its two-photon absorption spectrum with fluorescence quantum efficiency. The spectral peak represents the preferential excitation wavelength. When imaging multicolor probes concurrently, a wavelength compromise must be implemented to achieve balanced excitation efficiency across distinct spectral profiles. Pulse width is generally less than 100 femtoseconds (fs), with some systems achieving <70 fs to ensure high peak power and efficient two-photon absorption, while average power usually reaches the watt level to guarantee sufficient photon flux, and peak power can exceed 100 kW, a critical factor driving the nonlinear two-photon absorption process. Following attenuation through the microscope's optical pathway, the average power ultimately delivered to biological specimens typically resides within the range of 10–100 mW. Many systems support continuous wavelength tunability, facilitating the excitation of various fluorescent dyes or endogenous fluorescent molecules. Traditionally, Ti:Sapphire femtosecond lasers have dominated the market due to their broad tuning range and high stability, whereas newer systems are increasingly adopting all-fiber femtosecond lasers, which are more compact, easier to maintain, and suitable for miniaturized TPM.

The fundamental distinction between TPM and conventional single-photon microscopy lies in their fluorescence excitation mechanisms. In single-photon excitation, ground-state fluorescent molecules or atoms absorb a single photon upon laser irradiation, transitioning to an excited state before subsequently relaxing back to the ground state and emitting a fluorescent photon. By contrast, two-photon excitation involves the simultaneous absorption of two photons by ground-state fluorescent molecules or atoms within an extremely short timeframe (at the femtosecond scale), resulting in excitation to a higher energy state. During relaxation, a single fluorescent photon is emitted at a frequency slightly lower than twice that of the incident light [7]. Two-photon excitation is a nonlinear process that requires high light intensity, which restricts fluorescence emission strictly within a tiny volume at the focal point of the objective. This mechanism enables high-contrast 3D imaging without the need for a confocal pinhole, and reduces phototoxicity and photobleaching, making long-term in vivo observations over hours or even days possible. The fluorescence excitation process is schematically depicted in Figure 2. Table 1 gives a detailed comparison between TPM and conventional single-photon microscopy.

Table 1. Comparison of Two-Photon Microscopy and Single-Photon Microscopy.

Comparison Dimension	Two-Photon Microscopy	Single-Photon Microscopy
Sample Applicability	Thick tissues (e.g., brain slices, embryos, plant tissues) Living samples	Thin samples (e.g., single cells, tissue slices)
Excitation light	Long-wavelength (near-infrared)	Typically UV/visible light
Resolution Limit	~0.25 μm [8]	~0.25 μm [8]
Penetration Depth	Deeper (up to 1.6 mm) [9]	Shallower (typically <100 μm) [10]
Phototoxicity	Low	Higher
Optical Sectioning	Excellent (excitation only at focal plane, low background)	Requires confocal system; otherwise, low SNR
Signal-to-Noise Ratio (SNR)	High (low background)	Moderate in confocal mode, low in widefield

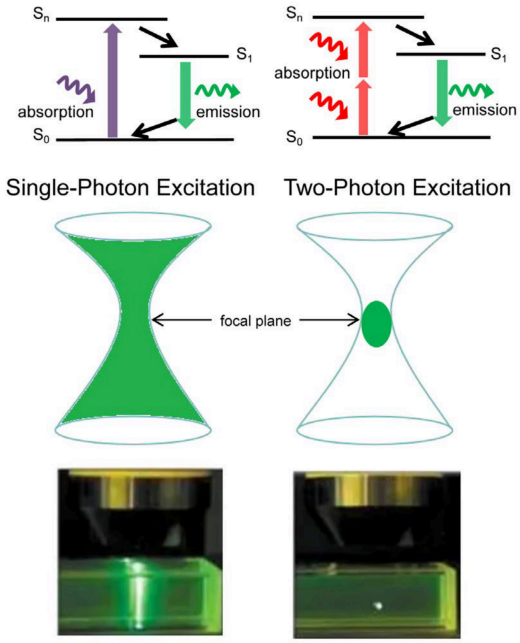

Figure 2. Excitation process in single (**left**) and two-photon (**right**) fluorescence microscopy.

3. Integration of Two-Photon Imaging with Other Technologies

In addition to the standard TPM, it can also be integrated with a multitude of emerging technologies to achieve novel imaging capabilities.

Combined TPM with super-resolution radial fluctuation (SRRF) [11], which analyzes random intensity fluctuations in time-series images to calculate the local radial gradient convergence property (termed "radiality"). This enables precise localization of emission centers, surpassing the diffraction limit to achieve super-resolution imaging at 120 nm. When combined with structured illumination microscopy (SIM) [12], the illumination light is modulated into periodic stripe patterns projected onto the sample. This "mixes" high-frequency information beyond the optical transfer function into detectable low-frequency regions. By capturing multiple raw images with varying stripe orientations and phases, algorithmic demodulation and reconstruction yield super-resolved images with a resolution of up to 89 nm. Coupling with stimulated emission depletion (STED) technology uses a superimposed excitation beam and a donut-shaped depletion beam to confine the fluorescent emission region below the diffraction limit via stimulated emission, pushing resolution further to <70 nm [13].

When integrated with optogenetics [14], a "read-write" closed-loop neural modulation system is achieved, enabling simultaneous high-resolution observation and precise neural control in live animals. Two-photon imaging serves as the "read" tool, using near-infrared femtosecond lasers to excite fluorescent calcium indicators, allowing real-time recording of neuronal activity at single-cell or even subcellular resolution. Optogenetics acts as the "write" tool, expressing light-sensitive proteins to achieve millisecond-scale activation or inhibition of specific neurons. Together, they enable closed-loop experiments within the same brain region—observe-intervene-reobserve—to precisely dissect causal relationships in neural circuits.

When coupled with adaptive optics (AO) [15], optical wavefront aberrations in TPM can be corrected to further enhance imaging quality. Biological tissues are complex 3D structures with heterogeneous refractive indices. As illumination or fluorescence light propagates through tissue, scattering and refraction induce wavefront distortions, leading to reduced resolution and contrast. These effects worsen with increasing imaging depth,

making AO increasingly critical. Currently, two main approaches exist: (1) Full AO [16]: uses a specialized wavefront sensor to measure aberrations and a wavefront corrector (e.g., deformable mirror or spatial light modulator) for compensation accordingly—fast but optically complex. (2) Sensorless AO [17]: lacks a separate wavefront sensor; instead, it iteratively optimizes the control signal of the corrector based on fluorescence signal intensity—simpler in setup but slower due to iterative optimization.

Integration with fluorescence lifetime imaging microscope (FLIM) [18] measures the average time a fluorophore remains in the excited state (fluorescence lifetime). This signal is independent of intensity and reflects the physicochemical microenvironment of the fluorophore. It enables 3D high-resolution imaging and label-free discrimination of endogenous fluorophores, with key applications in metabolic imaging [19–21] and sensing microenvironments (e.g., pH [22], membrane potential [23], temperature [24], ion [25], viscosity [26]).

Combined TPM with second harmonic generation (SHG) imaging [27], intense femtosecond lasers excite non-centrosymmetric structures in biological tissues, generating coherent radiation at twice the incident frequency (SHG signal). This process involves no photon absorption and exhibits minimal phototoxicity. As a label-free 3D imaging technique, it requires non-centrosymmetric targets and is widely used to image collagen [28] and myosin [29], showing promise for detecting early structural changes in diseases like diabetes [30] and cancer [31].

Combined TPM with coherent Raman imaging [32], another label-free modality is enabled. Two lasers (pump and Stokes) jointly excite molecular vibrations; when their frequency difference resonates with a specific chemical bond's vibrational frequency, coherent stimulated vibrations generate a strongly enhanced nonlinear signal. Unlike SHG, which reflects structural order without molecular specificity, coherent Raman imaging maps molecular composition with high chemical specificity, finding broad use in metabolic analysis [33], tumor identification [34], and drug development [35].

And integration with endoscopy [36] allows femtosecond pulses to be delivered via thin optical fibers to deep internal tissues, transforming two-photon imaging from a benchtop technique into a minimally invasive in vivo probe. Two-photon endomicroscopy leverages the intrinsic fluorescence of endogenous coenzymes, enabling visualization of organ microstructure [37] and monitoring of cellular metabolism [38] without exogenous dyes—applicable to tumor microenvironment analysis and cancer diagnosis.

The integration of TPM and photodynamic therapy [39], represents a cutting-edge frontier in biomedical optics, enabling integrated precision diagnosis and efficient treatment. By leveraging near-infrared femtosecond lasers and the principle of two-photon absorption, this technology achieves high-resolution imaging in deep tissues while simultaneously activating photosensitizers to generate reactive oxygen species (ROS) for precise tumor cell ablation. This synergistic approach overcomes the limitations of conventional photodynamic therapy—namely shallow penetration depth and limited treatment range—significantly enhancing diagnostic and therapeutic efficacy for deep-seated or solid tumors.

In fact, current multimodal imaging systems often integrate TPM with multiple other technologies (like FLIM and SHG) simultaneously to enhance the dimensionality of the acquired biological information [40,41], representing a major trend in TPM development.

4. Two-Photon Imaging in Neuroscience

In the long journey of neuroscience research, the 20th century was overwhelmingly dominated by electrophysiological recording techniques, which served as the primary research paradigm for deciphering neural activity at the time. However, the emergence of TPM in the 1990s brought a revolutionary breakthrough to the field, opening up a

new dimension for observing life [42]. By combining fluorescence labeling techniques, TPM enables us to explore the intricate morphological features of neurons, the complex synaptic connectivity networks, and the mechanisms of neural signal transmission with unprecedented precision (Table 2). This technology not only enables the fine observation of live cortical morphology and calcium ion dynamic imaging but also possesses the capability for long-term, real-time dynamic observation of freely moving animals. It can synchronously track the correlation between changes in cortical structure and function and behavioral characteristics. This technological breakthrough provides a powerful research tool for unraveling the working mechanisms of neural circuits and deciphering complex neurobiological phenomena, significantly expanding the boundaries of our understanding of the functional regulatory mechanisms of the nervous system.

Table 2. Neuron imaging with Two-Photon Microscopy.

	Imaging Target	Fluorescent Indicator	Example
Morphology	Axons; dendrites; spines	GFP/eGFP; YF	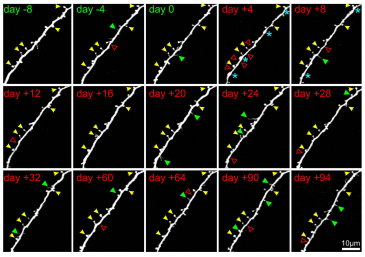 Chronic high-resolution imaging of dendritic spines with in vivo TPM. Reproduced with permission from Mostany, R. et al. [43]. Copyright 2021, Society for Neuroscience.
Neural signals	Ca^{2+}	Chemical (e.g., Indo −1, Fura −2, Fluo −4); 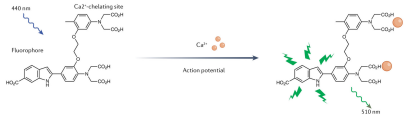 FRET-based GECI (e.g., TN-XXL); 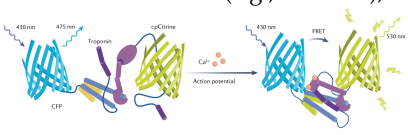 Circularly permuted GFP-based GECI (e.g., GCaMP6s). 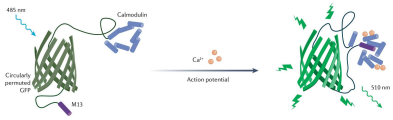 Copyright 2010, Springer Nature [44].	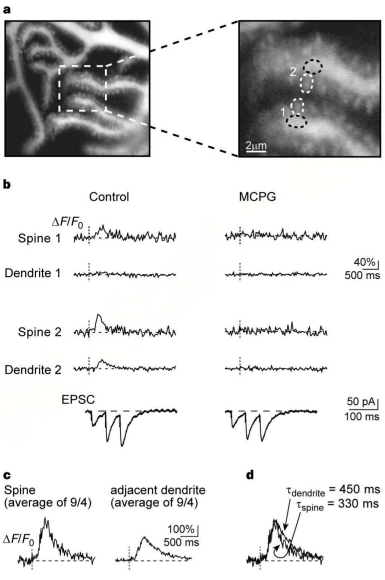 Calcium Imaging at the Synapse In Vitro. (a) Spiny dendrites of a Purkinje cell. (b) The dendrites shown in (a). (c) Averaged synaptic Ca^{2+} transients in pairs of spines and their adjacent dendrites. (d) Superposition of the normalized traces of (c). Reproduced with permission from Takechi, H. et al. [45]. Copyright 1998, Springer Nature.

Table 2. *Cont.*

	Imaging Target	Fluorescent Indicator	Example
Neural signals	NADH	NADH	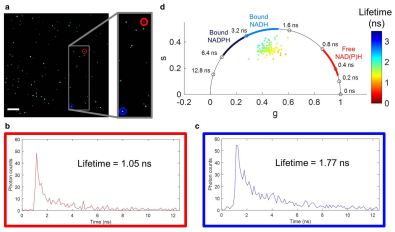 Heterogeneity of fluorescence lifetimes in extracellular vesicles (EVs) with TPM. (a) FLIM of EVs derived from MDA-MB-231 cells. (b) Example fuorescence decay curve of the EV in the red circle in (a). (c) Example fuorescence decay curve of the EV in the blue circle in (a). (d) Phasor plot of the frequency components of the exponential decays. Reproduced with permission from Sorrells, J.E. et al. [46]. Copyright 2021, Springer Nature.
	Glutamate	iGluSnFR	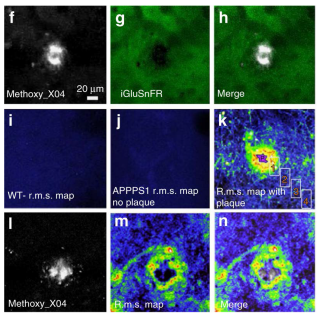 (f) Methoxy_X04-stained amyloid deposit. (g) iGluSnFR expression shown in green around the Ab plaque shown in f. (h) Merge of amyloid deposit and iGluSnFR. (i–n) Glutamate fluctuations were imaged using tplsm and are displayed in r.m.s. maps. Glutamate fluctuations were imaged. Reproduced with permission from Hefendehl, J.K. et al. [47]. Copyright 2016, Springer Nature.

4.1. Visualization and Functional Analysis of Neural Structures

The human brain orchestrates its functions through a staggering network of nearly 100 billion neurons interconnected by trillions of synapses in the central nervous system. This intricate communication system relies on precise information exchange between neuronal synapses, where visualizing these connections typically requires sub-micron spatial resolution. Dendritic spines, serving as the postsynaptic sites for most excitatory synapses in mammalian brains, have become focal points of modern neuroscience research.

The advent of high-resolution TPM and transgenic mice expressing fluorescent proteins has revolutionized the observation of these minute neuronal structures. For example, TPM enables: high-speed neural imaging at synaptic resolution [48], time-lapse imaging of dendritic spines in live cortical tissue across timescales from seconds to years [49], quantitative analysis of synaptic protein turnover and trafficking within these structures [50], live imaging of glial cells monitoring their microenvironment [51]. Long-term in vivo

two-photon imaging reveals that certain postsynaptic dendritic spines in adult cortex undergo rapid elimination or formation in response to altered sensory input or synaptic activity, which leads to experience/activity-dependent remodeling of neural circuits [23]. Under chronic pain conditions, peripheral injury triggers plastic changes in synaptic structure and function within the mouse somatosensory cortex [52].

The strength of excitatory synapses depends on both the amount of glutamate released and the number of postsynaptic receptors responding to glutamate. Using genetically encoded glutamate indicators like iGluSnFR, researchers can measure synaptic transmission in rodent organotypic slice cultures. Sparse labeling of pyramidal cells in hippocampal organotypic cultures enables TPM to image evoked glutamate transients [53]. Aerobic glycolysis serves as the primary glucose metabolic pathway in neuronal cell bodies, protecting neurons from oxidative damage. Miniaturized two-photon imaging reveals that the differential distribution of glycolytic enzyme pyruvate kinase M2 (PKM2) prompts neurons to utilize aerobic glycolysis in cell bodies for oxidative protection, while employing oxidative phosphorylation (OXPHOS) at synaptic terminals to meet high energy demands [54].

Affective empathy (AE), crucial for emotional transmission and maintaining healthy social relationships among mammals, has remained elusive in terms of its underlying neural circuitry. In 2024, Peng, S. et al. leveraged miniaturized two-photon imaging to demonstrate that two neural circuits originating from the ventral hippocampus are revealed to regulate naive observational fear. They further identified the naive observational fear encoding neurons in the ventral hippocampus. This groundbreaking work revealed multiple regulatory pathways of empathy in social animals and provided crucial insights into understanding empathy-related emotional disorders [55].

TPM has enabled comprehensive brain imaging ranging from neuronal structures to dendritic spines, and molecular analysis spanning from neuronal metabolic mechanisms to emotional empathy, establishing itself as a core tool for neural structural visualization and functional analysis. Despite revolutionizing in vivo brain imaging in mammals, its limitation to superficial cortical layers restricts observation of deeper brain regions. In 2025, Yang, M. et al. developed ULTRA (Ultra-wide, Layer-penetrating, Two-photon, Responsive Adaptive microscope), a novel TPM system featuring an ultra-large field of view (FOV > 50 mm^2) with single-cell resolution. By customizing optical components, integrating AO and high-performance PMT, this system achieved deep wide-field in vivo imaging across a 7 mm spatial range (from superficial cortex to 900 μm depth) with an imaging volume of 45.24 mm^3. This multifunctional platform overcomes traditional spatial constraints, enabling exploration of large-scale neural circuits at cellular resolution [56].

Additionally, conventional cranial windows for murine in vivo two-photon imaging face limitations in size and mechanical stability. Takahashi, T. et al. addressed this by creating large-scale cranial windows using flexible biocompatible polyethylene-oxide-coated CYTOP (PEO-CYTOP) nanosheets combined with photocurable resin. This technique supports multi-scale imaging in awake mice, ranging from subcellular structures to large-scale neural networks [57]. However, persistent challenges, including progressive window opacity over time, maintaining long-term transparency and preventing cerebral tissue desiccation, still urgently need to be addressed.

4.2. Real-Time Monitoring of Neural Signals

The pathways mediating information transmission between neurons are termed neural circuits. These circuits constitute intricate networks within brain regions, undergoing continuous dynamic remodeling that profoundly influences neuronal activity [58]. Intracellular calcium flux dynamics serve as a critical indicator of functional alterations in local cortical circuits [59]. When neurons generate action potentials, intracellular calcium ion

concentrations rise sharply. These calcium ions play a pivotal role in regulating complex signaling pathways within neurons, facilitating neurotransmitter release while maintaining long-term synaptic plasticity in dendritic branches and synaptic spines.

In vivo two-photon calcium imaging has emerged as a powerful technique for recording neuronal activity in intact brain tissue. Denk, W. et al. (1997) pioneered the TPM application for observing calcium dynamics in sensory-stimulated dendritic spines of pyramidal neurons in the mouse brain [42,60]. This breakthrough marked the beginning of widespread adoption of TPM in neuroscience research. This technique enables simultaneous acquisition of calcium transients at individual dendritic spines [61,62], while monitoring spontaneous or evoked activity from large neuronal populations at single-cell resolution [63,64].

Significant advancements include: Stosiek, C. et al. (2003) achieved in vivo Ca^{2+} imaging through intact skulls using membrane-permeable fluorescent indicators, capturing whisker-deflection-evoked transients in barrel cortex layer 2/3 neurons, enabling real-time analysis of intact neural circuits with cellular precision [65]. Grewe, B.F. et al. (2010) developed high-speed imaging resolving millisecond-scale action potential timing, revealing spatiotemporal variability in somatosensory and visual cortices [44]. Kim, T.H. et al. (2016) visualized neocortical dendritic morphology through sophisticated image stitching, accessing > 1 million neurons per mouse brain [66]. He, H. et al. (2021) demonstrated femtosecond-laser-mediated direct modulation of calcium channels, elucidating biochemical mechanisms underlying calcium influx induced by femtosecond laser irradiation [67].

TPM evolution has elevated imaging speeds to millisecond resolution while enabling precise capture of neuronal action potential sequences and exploration of calcium influx mechanisms. Current development focuses on deeper penetration [56,68], long duration [69,70], larger fields of view [71], miniaturization [72,73]. In 2025, Wu, R. et al. developed FHIRM-TPM 3.0, a 2.6 g miniature TPM capable of multicolor deep-brain imaging in freely behaving mice [74]. This system achieved: 10× adjustable FOV (max 1×0.8 mm^2) with 0.68–1.46 μm lateral resolution, neuronal imaging at a cortical depth of over 820 μm, calcium imaging with dendritic spine resolution in the hippocampus, dendritic spine-resolution hippocampal calcium imaging, and multi-color imaging revealing mitochondrial-cytoplasmic calcium dynamics relative to amyloid plaque deposition in awake mice. Despite these advances, challenges persist in clinical translation and deep-brain analysis. Maintaining high spatiotemporal resolution at greater depths remains critical, while multi-color imaging still faces limitations in spectral separation efficiency and phototoxicity control.

Although two-photon imaging has continuously made breakthroughs in the imaging depth and resolution of brain tissue, high-contrast deep tissue imaging that approaches or even reaches the optical resolution limit remains challenging due to optical aberrations and scattering introduced by dense biological samples. Therefore, combining super-resolution technology, optimizing optical design and correcting aberrations, and making breakthroughs in multicolor imaging technology are still the development directions for optimizing traditional TPM to address the trade-offs between imaging depth, duration, resolution, and FOV.

4.3. Research on Neurological Disease

TPM enables longitudinal identification of local neural circuits at the single-neuron level. This powerful technique has played a critical role in elucidating the underlying mechanisms of neurological disorders such as Alzheimer's disease (AD) and Parkinson's disease (PD), providing researchers with an unprecedented visualization tool to investigate disease progression.

AD is a prevalent and incurable neurodegenerative disorder, clinically characterized by progressive memory impairment, cognitive decline, personality alterations, and neuropsychiatric symptoms including language deficits. The etiology and pathogenesis of AD are not yet fully understood. Its hallmark pathological features include extracellular senile plaques composed of β-amyloid deposits and intracellular neurofibrillary tangles formed by hyperphosphorylated tau protein [58]. Skoch, J. et al. employed TPM through cranial windows to label and longitudinally monitor β-amyloid deposition in mouse brains [75]. In AD mouse models, dendrites and axons near amyloid plaques exhibited characteristic neurite disruption, dendritic spine loss, axonal atrophy, and degeneration [76]. Progressive cytoskeletal disorganization within neurites became evident within days after plaque deposition [77]. Notably, axonal dystrophies near A β-plaques were observed in vivo through continuous two-photon imaging over 200 days in both 7-month-old dE9 and 3-month-old APP-PS1 mice, which represent early stages of amyloid pathology [78]. In vivo two-photon calcium imaging revealed how A beta and tau synergize to impair the functional integrity of neural circuits and suggest a possible cellular explanation contributing to disappointing results from anti-A β therapeutic trials [79]. The capacity to monitor these AD hallmarks in real-time facilitates the evaluation of therapeutic and preventive strategies.

PD is a complex disorder clinically manifested by motor deficits such as tremor, bradykinesia, and rigidity, along with cognitive impairment. Traditionally, it has been primarily associated with pathological changes in the midbrain (substantia nigra and striatum). Postmortem studies have proposed that the structural changes in dendrite spines in medium spiny neurons may contribute to late-stage motor complications of PD [80]. In vivo two-photon imaging shows that in 1-Methyl-4-phenyl-1,2,3,6-tetrahydropyridine (MPTP)—induced PD mouse model, dendritic spine elimination and formation increase in the motor cortex, regulated by D1 and D2 dopamine receptors, respectively [81]. A key pathological feature of PD involves the abnormal accumulation and proliferation of α-synuclein. Two-photon in vivo imaging enables real-time observation of α-synuclein accumulation at neocortical synapses, with evidence suggesting that reducing this synaptic accumulation alleviates PD symptoms [82]. Olfactory dysfunction is an early symptom of PD. Studies show reduced neuronal survival rates and decreased dendritic spine density in the olfactory bulb of A30P α-synuclein transgenic mice overexpressing α-synuclein. Additionally, two-photon in vivo imaging detected altered neural activity patterns in the barrel cortex of α-synuclein-overexpressing transgenic mice [83].

5. Two-Photon Imaging in Immunology

Immunology is the scientific discipline dedicated to investigating the structural organization and molecular composition of the immune system, elucidating the intricate processes and regulatory mechanisms underlying immune responses, and deciphering the resultant effector functions. Within this complex system, immune cells orchestrate a cascade of events including pathogen recognition, activation, proliferation, differentiation, and execution of effector functions. These processes collectively enable the body to deploy robust immune defenses against infections, facilitate clearance of senescent cells, maintain inflammatory homeostasis through immune cell regulation, and conduct continuous immune surveillance to prevent cellular transformation [84]. A critical challenge in immunological research stems from the deep-seated localization of lymphocyte functions within dense lymphoid organs. Specifically, antigen recognition and other cellular interactions occur in anatomical regions that preclude direct in vivo observation. Consequently, the dynamic interplay between immune cells has historically been inferred through in vitro experimental models [84].

In conventional immunological imaging, laser scanning confocal microscopy enables visualization of innate immune cell populations (e.g., monocytes and macrophages) in murine models. However, this technique faces fundamental limitations due to light scattering effects, which restrict tissue penetration depth and compromise imaging resolution in deep tissues [85]. TPM overcomes these constraints through innovative optical principles and achieves superior tissue penetration while minimizing phototoxic effects compared to conventional imaging modalities. This technological advancement enables direct visualization of immune cell dynamics in live tissue with unprecedented depth and temporal resolution [85,86].

Over the past two decades, TPM has been instrumental in advancing immunological research across diverse domains (Table 3). Its applications span from fundamental studies of lymphocyte development and immune cell activation to investigations of intercellular communication networks and effector cell-target cell interactions. The technique has also been pivotal in elucidating immune homeostasis mechanisms, deciphering pathological processes in infectious and autoimmune diseases, characterizing tumor microenvironment components, and elucidating the mechanisms of action for immune-modulating therapeutics. Collectively, these technological breakthroughs provide a robust experimental framework for deciphering the cellular orchestration of immune responses at unprecedented spatiotemporal resolution.

Table 3. Immune cell imaging with Two-Photon Microscopy.

Cell Type	Target	Key Findings	Image with TPM	Refs.
Neutrophils	Ly6G	Uncover the cascade processes of neutrophil extravasation and their biological functions in migration; elucidate their distinct inflammatory characteristics across different pathological phenotypes.	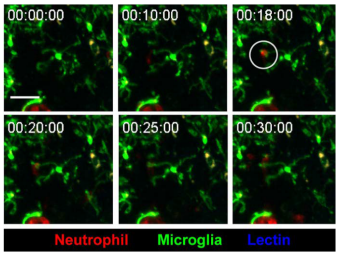 Crosstalk between microglia and neutrophils in inflamed brain parenchyma Reproduced with permission from Kim, Y.R. et al. Copyright 2020, Frontiers Media S.A. [87]	[87–90]
Macrophage	M1 (CD40, CD86) M2 (CD206, CD200R) NADH and FAD	Tracking the metabolic activity, cellular responses, and polarization behavior dynamics of different macrophage subtypes in disease models.	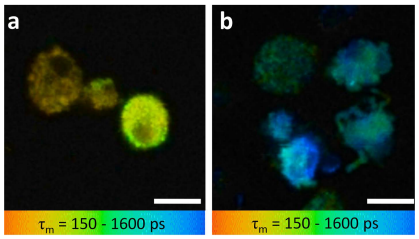 Image of monocyte-derived M1-polarized (IFN-γ) MΦs (**a**), monocyte-derived M2-polarized (IL–4) MΦs (**b**) Reproduced with permission from Kröger, M. et al. Copyright 2022, eLife Sciences Publications Ltd. [91]	[91–93]

Table 3. *Cont.*

Cell Type	Target	Key Findings	Image with TPM	Refs.
T cell	CD4 CD8 CFSE Ca^{2+}	Visualizing T-cell activation processes within the body reveals the underlying causes of inflammation.	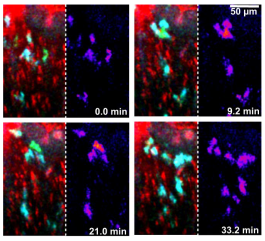 Calcium signaling of OVA-specific T cells in the ileal LP Reproduced with permission from Bauer, I.J. et al. Copyright 2023, National Academy of Sciences. [94]	[94]
B cell	CD19 GL7	Visualization of B cells in virus-infected mouse lungs reveals the spatiotemporal mechanisms of cellular activation.	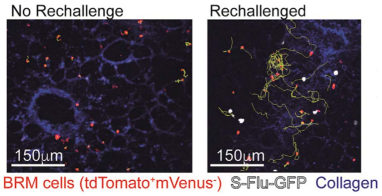 Lung-resident memory B cells increase motility following rechallenge Reproduced with permission from MacLean A.J. et al. Copyright 2022, Elsevier. [95]	[71,95]
DC	CD11c	The migration of DC in the interstitial space as well as their interactions with adaptive immune cells.	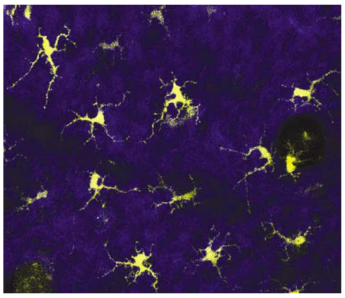 Two-photon image of LC within ear skin of a CD11c-EYFP mouse (yellow) Reproduced with permission from Cavanagh, L.L. et al. Copyright 2008, Springer Nature. [96]	[96]
NK	CD27 (bone brown) CD11b (spleen)	Mature NK cells continuously patrol the bone marrow to respond to systemic viral challenges and rapidly proliferate.	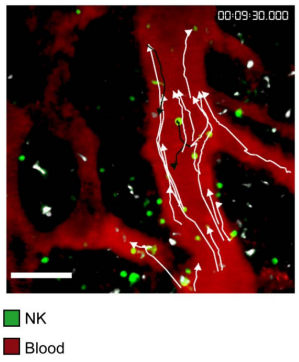 NKs were tracked crawling and rolling in a blood vessel in the BM. Reproduced with permission from Milo, I. et al. Copyright 2018, Wiley. [97]	[97]

5.1. Dynamic Observation of Immune Cells

Owing to its unparalleled advantages in deep tissue imaging and in vivo observation, TPM was rapidly adopted by immunologists in the early 21st century to investigate cellular functional dynamics within intact organisms. This technological leap fundamentally transformed our capacity to interrogate the spatiotemporal behavior of immune cells in their native environments [64].

In 2002, Miller, M.J. et al. pioneered TPM visualization of the motility of individual live lymphocytes deep within intact lymph nodes. Their findings revealed that T cells exhibited peak velocities exceeding 25 μm/min, with a motility coefficient 5–6 times higher than that of B cells. Real-time TPM imaging provided critical insights into immune response initiation dynamics [98]. Thymocyte maturation relies on selection based on interactions with self-major histocompatibility complex (MHC)-peptide complexes presented by thymic stromal cells. Using TPM, Bousso, P. et al. performed real-time analysis of cell contacts in 3Dthymic organ cultures during positive selection. The study demonstrated the diversity and dynamism of thymocyte interactions, revealing that a significant proportion of thymocytes exhibit high motility in culture. Notably, MHC recognition prolonged thymocyte-stromal cell contact durations, promoting stable cell–cell interactions essential for positive selection [99]. Celli, S. et al. developed a protocol to visualize lymph node T cell behavior during initial activation or tolerance induction in anesthetized mice, offering novel insights into lymphocyte migration and intercellular communication [100].

In vivo two-photon imaging elucidated how the microbiota influences T cell responses as triggers of central nervous system inflammation. Researchers visualized the activation of encephalitis-derived $CD4^+$ T cells in the ileal lamina propria, linking gut microbiota composition to autoimmune pathogenesis [94]. $CD4^+$ T helper cells play a central role in combating intracellular pathogens. Filipe-Santos O. et al. observed the behavior of pathogen-specific CD4 T cells with TPM at the site of Leishmania major infection, revealing that disparities in the dynamics of T cell contacts with infected cells and local variation in T cell access to infected cells are important elements of the host–pathogen interplay [101]. TH17 cells are a highly plastic subset of T cells that play a crucial role in autoimmunity. Loos, J. et al. tracked TH17 cell dynamics with TPM in an experimental autoimmune encephalomyelitis (EAE) model, highlighting their effector functions in neuronal dysfunction [102]. The immunosuppressive role of regulatory T cells (Tregs) has been extensively studied using TPM. In vivo analyses demonstrated that Tregs exert their function by limiting T helper (Th) cell access to dendritic cells (DCs), Th cell arrest and their prolonged contacts with DCs are progressively inhibited with increasing number of Tregs, and the reduced DC contacts are associated with suppressed proliferation and differentiation of Th cells. [103]. With a hepatitis B virus (HBV) mouse model, Guidotti L. et al. demonstrated how circulating CD8 Tregs homing to the liver recognize antigens and deploy effector functions, unveiling dynamic control mechanisms against liver-tropic pathogens [104]. Combining classical immunological approaches with TPM, Qi H's group discovered a novel mechanism by which BCL6 regulates humoral immunity: BCL6 modulates follicular helper T cell interactions with B cells through calcium signaling, helping maintain T helper cell phenotypes in a T cell non-autonomous manner [105]. Conventional point-scanning TPM enables tissue imaging at 1 mm depth but suffers from slow speed and high phototoxicity. In 2023, the team led by Dai, Q. at Tsinghua University developed a two-photon synthetic aperture microscopy that achieved continuous 3D imaging in live mice for tens of hours. This breakthrough enabled the first complete recording of the formation process of lymph node germinal centers (GC), revealing a B-cell proliferation-dominated mechanism for GC formation [71]. The imaging throughput was enhanced by three orders of magnitude while reducing phototoxicity by over 1000-fold.

DCs serve as central regulators of immune responses. Current characterization of DC function primarily relies on static analysis of ex vivo isolated cells or immunohistochemistry. In vivo TPM enables real-time investigation of DC behavior within intact tissue contexts, revealing distinct lymph node activities under both homeostatic and inflammatory conditions [96]. Compared to antigen-naive DCs, antigen-specific T cells engage in prolonged interactions with antigen-loaded DCs. TPM imaging has detailed the temporal dynamics of DC-T cell interactions during lymph node activation [106,107]. Macrophages (MΦs) are crucial immune effector cells that can either promote or suppress inflammation and participate in diverse physiological and pathogenic immune responses. Kröger, M. et al. utilized two-photon excitation FLIM—a label-free, non-invasive technique—to visualize human dermal MΦs in vivo, observing their phenotypes and phagocytic activities to enhance understanding of MΦs roles in health and disease [91]. Two-photon imaging of human MΦs following pro-inflammatory or anti-inflammatory stimuli enabled the determination of optical redox ratios of coenzymes flavin adenine dinucleotide (FAD) and nicotinamide adenine dinucleotide (NADH) involved in key metabolism, along with mitochondrial clustering patterns, thereby tracking dynamic changes in macrophage metabolism [108]. Using two-photon fluorescence probes, real-time imaging and tracking of macrophage migration inhibitory factor (MIF) within cells has also been achieved, establishing correlations between MIF fluctuations and fluorescence signal changes during cancer progression [109].

Challenges still remain in two-photon imaging for immune cells, including limited FOV, insufficient imaging depth, and difficulty in labeling and distinguishing specific cell types or functional subsets. Currently, immune cell observation primarily relies on fluorescent protein labeling, which however may affect the normal activity and function of immune cells over long-term tracking. Label-free microscopic imaging, which utilizes the intrinsic fluorescence of naturally metabolized proteins under two-photon excitation, has emerged as an ideal tool for in vivo imaging. Yet, this method struggles to accurately differentiate immune cell subtypes, suffers from weak signal intensity, and is prone to tissue background interference, making long-term dynamic tracking of specific immune cells difficult. Recently, Kreiss, L. et al. applied a deep learning approach to a dataset of label-free microscopic images from diverse immune cell types, enabling direct detection of specific immune cells in unlabeled images, thereby enhancing the specificity of label-free imaging through computational means [110].

5.2. Depth Analysis of Immune Response

TPM enables high-resolution observation of immune response processes, which is crucial for deepening our understanding of immune response mechanisms [111]. Neutrophils, once regarded as simple frontline warriors of the innate immune system, are now recognized as complex cells with multiple specialized functions. As effectors of innate immune responses, they regulate numerous processes, including acute injury and repair, cancer, autoimmunity, and chronic inflammatory processes [112].

Following infection or injury, neutrophils rapidly extravasate from blood vessels. Once exiting the vasculature, individual neutrophils typically exhibit highly coordinated chemotaxis and swarm-like clustering behavior. Using two-photon in vivo imaging, Palomino-Segura, M. et al. described neutrophil extravasation and cellular dynamics within the tracheal tissue of Streptococcus pneumoniae-infected mice [113]. In germ-free mouse models of injury and infection, Lämmermann, T. et al. used TPM to demonstrate the critical role of leukotriene B4 in mediating intercellular signaling between neutrophils, where aggregated neutrophils reorganize the dermal collagen fiber network to form compact cell clusters [114]. Within bone marrow, the response of neutrophil to hematopoietic cytokine granulocyte colony-stimulating factor (G-CSF) also relies on collective migration. Using TPM, Kohler,

A. et al. demonstrated that G-CSF rapidly induces the motility and entry of neutrophils into blood vessels, a network of signaling molecules, chemokines, and cells controls neutrophil release from the bone marrow, and their mobilization involves rapidly induced Cxcr2-mediated motility controlled by thrombopoietin as a pacemaker [115]. Neumann, J. et al. also observed increased interactions between neutrophils and microglia following very-late-antigen-4 (VLA-4)-mediated brain invasion during ischemic injury [116].

Beyond elucidating distinct neutrophil-specific mechanisms, in vivo TPM is well-suited for investigating more fundamental cellular processes. Recent studies indicate that ion efflux during endocytosis is a necessary mechanism for MΦs to regulate extracellular fluid uptake [117]. In vivo TPM demonstrated that MΦs can rapidly infiltrate sterile tissue injuries in visceral organs via non-vascular pathways. In a sterile liver injury model, peritoneal macrophage recruitment occurs through direct migration from the peritoneal cavity and depends on ATP and CD44. This mechanism, diverging from classical vascularized recruitment pathways, significantly accelerates macrophage accumulation at injury sites, thereby facilitating faster recovery [118]. Using supercontinuum-truncated TPM (SCT-TPM) technology, the spatiotemporal dynamics of clonally heterogeneous tumor evolution can be visualized in live tumor-bearing mouse models. Simultaneous imaging of multiple fluorophores within the tumor microenvironment enables observing key biological events such as immune cell engulfment and killing of tumor cells, tumor cell lysis, and vesicle secretion. This reveals distinct behaviors of tumor subclones during the tumor-host interaction [119].

5.3. Immunotherapy

The remarkable clinical successes of tumor immunotherapies achieved in recent years—including tumor-targeting monoclonal antibodies, immune checkpoint inhibitors, and chimeric antigen receptor T-cell (CAR-T) therapies—have created an urgent need to understand their precise mechanisms of action within patients. In vivo two-photon imaging provides unique insights into the operational dynamics of these therapies and helps identify critical bottlenecks. By observing changes in the distribution and function of immune cells within the tumor microenvironment before and after treatment, researchers can more accurately assess the efficacy of immunotherapy. Functional in vivo two-photon imaging within the tumor microenvironment enables dynamic monitoring of phagocytosis by labeling MΦs and tumor cells with pH-sensitive probes. Introducing the caspase-3 reporter gene into tumor cells allows monitoring of tumor cell killing mediated by cytotoxic T lymphocyte (CTL) or CAR-T. Additionally, the calcium ion reporter gene expressed by T cells provides single-cell intracellular signaling information during tumor-T cell interactions. And nuclear translocation of fluorescent STAT-1 fusion proteins enables tracking of interferon signaling [120]. Membrane damage during tumor-CTL interactions can be inferred from elevated calcium ion concentrations in tumor cells.

Real-time imaging of the gastrointestinal tract using TPM has proven to be a valuable tool for mucosal immunologists. Its ability to penetrate deep into living tissue while minimizing phototoxicity and photobleaching makes it particularly adept at deciphering dynamic immune processes involving cell movement that persist for minutes to hours [121]. CAR-T immunotherapy is considered one of the most promising approaches in cancer treatment. Ma, B. et al. prepared biocompatible and mass-producible polydopamine (PDA) nanodots. Under ambient pressure and room temperature conditions, PDA and hydrogen peroxide react to synthesize oxidized polydopamine (OPDA) nanodots exhibiting both single-photon and two-photon fluorescence properties. Combined with TPM, OPDA nanoparticles enable long-term imaging of live cells without inhibiting division or proliferation. OPDA-labeled Raji cells can be visually assessed via fluorescence to validate the lethality and efficacy of CAR-T. Due to different ROS concentrations between malignant

and normal cells, fluorescence intensity changes from PDA to OPDA conversion provide a tumor-specific fluorescence signature [122]. Despite clinical efficacy for certain cancers, the mechanism of anti-PD-1 monoclonal antibodies (aPD-1) remains incompletely understood. In 2017, intravital imaging by Arlauckas, S.P. et al. revealed rapid binding of aPD-1 to PD-1$^+$ tumor-infiltrating CD8$^+$ T cells in mice, followed within minutes by capture via PD-1- tumor-associated MΦs. This Fcγ receptor-dependent uptake—contingent on antibody glycosylation—can be prevented by Fcγ receptor blockade, prolonging CD8$^+$ T cell engagement and enhancing tumor regression. These studies provide insight into aPD-1 target engagement in vivo and identify specific Fc/Fcγ receptor interactions that can be modulated to improve checkpoint blockade therapies [123].

In 2023, Wang, L. et al. reported a mitochondrial-targeting iridium (III) complex Ir-pbt-Bpa as an efficient immunogenic cell death-inducing photosensitizer for two-photon photodynamic immunotherapy against melanoma. Following irradiation, Ir-pbt-Bpa not only induces CD8$^+$ T cell responses and regulatory T cell exhaustion but also increases effector memory T cell numbers, enabling sustained antitumor immunity [124]. In 2025, Tan, Y. et al. developed a two-photon photosensitizer (TPSS) that targets tumor-overexpressed carbonic anhydrase IX (CA IX). Under two-photon laser excitation, TPSS generates a large amount of ROS, inducing immunogenic cell pyroptosis and triggering a robust antitumor immune response, further highlighting the promising prospects of TPSS in cancer therapy [125].

6. Two-Photon Imaging in Oncology

TPM enables deep-tissue biological studies within tumors at single-cell resolution, detecting signaling status, tumor invasion, and immune cell dynamics [126]. This allows researchers to monitor tumorigenesis, metabolism, metastasis, and treatment responses at the cellular level, significantly enhancing the understanding of cancer biology and therapeutic responses.

6.1. Imaging of Cancer Cells and Tissues

Histopathological examination using hematoxylin and eosin (H&E) staining remains the gold standard for cancer diagnosis. With ongoing advances in TPM, this technique emerges as a promising alternative to traditional histopathological processing and analysis, offering faster, real-time capabilities. In ex vivo human gastrointestinal mucosal samples, Rogart, J.N. et al. utilized intrinsic fluorescence signals for TPM imaging, demonstrating structural details comparable to H&E-stained sections while achieving superior imaging performance [127]. Similar conclusions were drawn from comparative analyses of TPM-imaged human ovarian biopsies (normal and neoplastic) with corresponding H&E-stained tissues. Furthermore, the discrimination between normal and neoplastic tissues can be done by detecting red shift in cellular intrinsic fluorescence and collagen structural alterations in preclinical mouse models of ovarian cancer in vivo [128]. Subsequent studies have expanded TPM for tissue discrimination across various cancers including gastric, thyroid, prostate, and oral carcinoma [129–132].

Beyond differentiating normal and malignant tissues, label-free TPM enables rapid visualization of multiple tumor microenvironment alterations, including fibrotic responses, inflammatory cell infiltration, mucinous reactions, and isolated residual tumor cells. This capability facilitates assessment of tumor regression and stromal responses. Concurrently, computational image analysis can extract collagen morphological features as optical imaging biomarkers for distinguishing pathological tissue [133,134]. These findings suggest TPM's potential for real-time in vivo pathological diagnosis and as an adjunct tool for evaluating neoadjuvant therapy responses.

Early TPM imaging of neoplastic tissues primarily relied on endogenous fluorescent molecules. However, weak signal and poor contrast in deep tissues due to background interference result in failing to achieve tumor-specific precise imaging [126,135]. Consequently, developing bright, tumor-targeted, biocompatible exogenous fluorescent probes is essential for deep-tissue in vivo tumor imaging. Kong, X. et al. developed a unique red-emitting two-photon probe (N-BN) using Nile Red as the fluorophore and employed biotin as a tumor-targeting ligand. This probe enables specific imaging of biotin receptor-positive cancer cells via two-photon excitation. In vivo, N-BN-loaded tumor tissue exhibited strong red two-photon fluorescence signals with a penetration depth of ~90 μm. Furthermore, N-BN could also track the tumor with highly tumor-specific properties in a near-infrared manner [136]. Liu, Y. et al. created a two-photon probe responsive to nitroreductase (NTR) for detecting hypoxic microenvironments in cancer stem cells (CSCs) in vitro and in vivo. Two-photon absorption cross-section extends fluorescence excitation into the near-infrared range, significantly enhancing tissue penetration for hypoxic CSC detection [137]. Zha Y. et al. encapsulated near-infrared II (NIR-II) fluorophores within DSPE-PEG to create biocompatible, rapidly metabolized two-photon nanoprobes. These probes were efficiently internalized by cancer cells, enabling clear tumor imaging [138]. NAD(P)H: quinone oxidoreductase 1 (NQO1) plays a role in intracellular free radical reduction and detoxification and has been linked to colorectal cancer and chemotherapy resistance. Jiang, W. et al. developed a novel two-photon fluorescent probe, WHFD, which is capable of selectively detecting intracellular NQO1 in tumor-bearing mice and human colorectal cancer specimens at depths up to 300 μm. This probe demonstrated reliable diagnostic performance for direct in situ biomarker imaging and a clear distinction of tumor margins [139]. Hao, L. et al. employed a co-crystallization strategy to develop the two-photon absorbing material BP4TC and its water-dispersible nanoparticles (BP4TC-NPs). Under 900 nm excitation, BP4TC-NPs produced bright, low-background fluorescence in human A549 lung cancer cells with negligible cytotoxicity [140].

6.2. Deciphering Tumor Metabolism

Rapid, sensitive, and non-invasive assessment of cellular metabolism is a critical need in biomedicine. The intensity and fluorescence lifetime properties of endogenous coenzymes NAD(P)H and FAD serve as vital biomarkers for characterizing cellular metabolic states in living biological tissues. Tumor cells typically exhibit elevated free NADH levels, increased protein-bound FAD, and a higher reduction-oxidation ratio, corresponding to a hyperglycolytic phenotype, whereas normal tissues primarily rely on OXPHOS [141,142]. Due to the unique advantages in label-free, deep-tissue, single-cell resolution metabolic characterization, two-photon FLIM has become a cornerstone tool for tumor metabolism research. Bird, D.K. et al. utilized this technique to measure the fluorescence lifetime and ratio of free versus protein-bound NADH, enabling in vivo mapping of the intracellular reduction-oxidation ratio. This approach revealed distinct metabolic features in cancer cells, such as in MCF10A and Hs578T cell lines [143,144]. Subsequent studies confirmed that the shortened fluorescence lifetime of bound NADH serves as a diagnostic marker for cancer [145]. In 2019, Cong, A. et al. employed 2P-FLIM to detect endogenous NAD(P)H, comparing metabolic profiles and responses to targeted metabolic compounds in 4T1 murine breast cancer cells cultured in 2D versus 3D collagen matrix. This work reveals that integrating 2P-FLIM of intrinsic NAD(P)H with refined 3D tumor-matrix in vitro models promises to advance our understanding of the roles of metabolism and metabolic plasticity in tumor growth and metastatic behavior [146]. Leveraging advances in artificial intelligence, machine learning algorithms have been integrated with 2P-FLIM to statistically analyze single-cell redox states based on endogenous NAD(P)H and FAD autofluorescence.

This approach tracked metabolic changes in live cancer cells under doxorubicin treatment, confirming the utility of single 800 nm wavelength excitation for dual-coenzyme metabolic imaging and demonstrating the robustness of machine learning analysis [147]. To unlock the clinical potential of FLIM, Liang W. et al. developed a miniaturized two-photon FLIM endoscope system. With an approximate 2 mm diameter, subcellular resolution, and high photon collection efficiency, this system successfully tracked NADH lifetime dynamics during apoptosis induction in cultured cancer cells and subcutaneous mouse tumor models. By providing complementary structural and metabolic information, it enables label-free in situ functional histology of organs, offering a novel tool for clinical diagnostics [148].

Compared to normal cells, cancer cells contain elevated levels of metabolites like glutathione (GSH) and hypochlorous acid (HClO), making them potential biomarkers for tumor imaging. GSH is crucial for maintaining cellular redox homeostasis. A coumarin derivative-based two-photon probe, Cou-Br, was developed for GSH detection in live cells, mouse models, and clinical specimens. It successfully identified human laryngeal carcinoma lesions, demonstrating excellent deep-tissue imaging and tumor margin delineation capabilities [149]. Another probe, TPEF-GSH, enabled quantitative visualization of intracellular GSH in vivo, reflecting tumor redox status [150]. Two-photon probes (Biotin-HClO and HDM-Cl-HClO) were developed for real-time HClO monitoring in inflammation and tumor mouse models, facilitating high-contrast tumor imaging by distinguishing neoplastic from normal tissue [151,152]. Ferroptosis regulates cell death via ROS accumulation-related lipid peroxide accumulation, affecting lipid droplet (LD) structure and polarity. The polarity-sensitive two-photon probe LIP-Pola, featuring LD-anchoring capability, enabled in situ imaging analysis of ferroptosis via LD polarity changes in tumor cells and tissues [153]. In 2024, Wu, T. et al. pioneered the use of tryptophan (Trp) for probing cellular metabolism with two-photon FLIM. In vitro cell experiments successfully distinguished tumor cells from healthy cells based on Trp fluorescence lifetime, tracked the efficacy of the immunotherapeutic agent 1-MT on HeLa cells, and monitored cellular responses to carbonyl cyanide 3-chlorophenylhydrazone-induced apoptosis [154]. These results establish metabolite-based two-photon autofluorescence lifetime as a sensitive natural probe for live-cell metabolism and a valuable analytical tool for in vivo tumor imaging.

6.3. Tumor Vasculature Imaging

During tumor growth, the release of pro-angiogenic cytokines recruits new blood vessels to grow into the tumor, inducing the formation of tumor neovasculature. This process provides essential blood supply and nutrients for the growing tumor and is a hallmark feature of cancer. Visualizing the vascular system is crucial for understanding disease onset and progression [155,156]. Two-photon absorption near-infrared fluorescent probes conjugated with RGD (L-arginine (R), glycine (G), and L-aspartic acid (D) residues) exhibit specific targeting capability toward tumor vasculature, enabling high-resolution tumor vascular imaging. In Lewis lung carcinoma (LLC) tumors, this approach has achieved 3D imaging of the tumor vascular system at a depth of up to 830 μm, with excellent contrast [157,158]. Additionally, a near-infrared fluorophore BTPETQ with aggregation-induced emission (AIE) characteristics shows enhanced two-photon fluorescence under 1200 nm (NIR-II) excitation. It enables deep 3D imaging of the mouse cerebral vascular network up to 924 μm, and can clearly distinguish between normal and tumor vessels in deep tumor tissues (over 900 μm) with high SNR [159]. These studies demonstrate the significant value of TPM in tumor vasculature imaging.

6.4. Invasion and Metastasis

Tumor invasion and metastasis are common in cancer and significantly limit patient prognosis. TPM allows 3D visualization and quantification of early invasive behaviors of tumor cells at primary sites [130,160]. By using two-photon laser ablation, 3D microtracks can be generated within dense 3D collagen matrices, which guide collective invasion independently of pericellular proteolysis [161]. Zhang, W. et al. combined a chronic cranial window with TPM to establish a syngeneic orthotopic cerebral metastasis model in mice. This setup enables long-term, single-cell-level in vivo tracking of fluorescently labeled tumor cells and tumor-associated macrophages/microglia (TAM/M), and analysis of the role of their receptor CX3CR1 in different stages of brain metastasis formation from lung cancer [162]. This technique also allows investigation of the in vivo dynamics and antitumor effects of epithelial cell adhesion molecule-directed CAR T cells against brain metastases from lung cancer [163]. Furthermore, by optimizing the excitation wavelength to simultaneously excite FAD and NAD(P)H, robust quantitative optical biopsy of hepatocellular carcinoma and its metastases can be achieved in situ based on two-photon autofluorescence imaging.

6.5. Two-Photon Photodynamic Therapy for Cancer Cells

Surgery, radiotherapy, chemotherapy, and immunotherapy remain the conventional pillars of cancer treatment. In recent years, photodynamic therapy (PDT) has emerged as a highly promising novel modality due to its precise spatiotemporal selectivity and non-invasive nature. Its therapeutic efficacy, however, is typically constrained by local oxygen concentration and penetration depth. Two-photon photodynamic therapy (TP-PDT) offers an innovative solution by simultaneously absorbing two near-infrared photons to activate photosensitizers, thereby generating ROS for targeted cancer cell ablation [164]. Compared to PDT, TP-PDT has deeper tissue penetration, higher spatial selectivity, and superior treatment safety.

In early 1997, Bhawalkar, J. et al. demonstrated the feasibility of combining infrared excitation, efficient two-photon absorbing dyes, and photosensitizers in PDT [165]. Since then, extensive in vitro and in vivo studies have been conducted across multiple cancer types. A range of photosensitizers—including pyropheophorbide-α methyl ester (MPPa) [166], iridium complexes [167], sulfonated aluminum phthalocyanine (AlPcS) [168], water-soluble porphyrin self-assemblies [169], and triphenylamines (TPAs) [170]—have demonstrated potent cytotoxic effects under two-photon excitation within the 750–1200 nm NIR window. These agents have validated their potential in models of cervical, lung, ovarian, and nasopharyngeal cancers and HeLa cells, laying critical experimental foundations for subsequent in vivo studies and clinical translation.

TPAs selectively localize to cellular organelles (primarily mitochondria) and, under two-photon excitation (760–860 nm), generate substantial ROS to rapidly initiate apoptosis [170]. The TiO_2-CUR-Sofast (TCS) composite, formed by modifying curcumin (CUR) with titanium dioxide nanoparticles and Sofast cationic polymer, exhibits enhanced photosensitizing potential under visible light. Under NIR irradiation, TCS produces 6–7 times more ROS than CUR alone. In TP-PDT experiments, TCS demonstrates significantly higher phototoxicity against HeLa and T24 cell lines; with 900 nm irradiation, approximately 89% of TCS-treated cells undergo apoptosis or necrosis, confirming its superior therapeutic efficacy [171]. TPSS, specifically targeting overexpressed CA IX on tumor cells, exhibits exceptional tumor selectivity. Upon two-photon activation, TPSS generates abundant ROS, inducing pyroptosis and triggering a robust anti-tumor immune response [125]. RGD peptide-conjugated ruthenium(II) complexes selectively target the mitochondria of integrin $\alpha_v\beta_3$-rich tumor cells, enabling precise tumor ablation [172]. Due to the hypoxic microenvironment in solid tumors, oxygen-independent photosensitizers

are urgently needed. An iridium(III)-anthraquinone complex localized to mitochondria acts as a carbon radical initiator, inducing mitochondrial membrane potential collapse and cell death even under anoxia—marking the first metal-complex-based theranostic agent for oxygen-independent TP-PDT [173]. These advances collectively underscore the transformative potential of TP-PDT in oncology.

Despite the unique advantages of TPM in tumor diagnosis, metabolism, angiogenesis, invasion, and therapy, deep-tissue penetration remains a fundamental limitation. Comprehensive imaging of deep-seated solid tumors and distant micrometastases remains an unresolved challenge. Furthermore, the development of tumor-specific two-photon probes requires further refinement. The persistent hypoxic tumor microenvironment continues to drive the urgent need for oxygen-independent photosensitizers. With the ongoing evolution of multimodal two-photon technologies and the rational design of safe, non-toxic, in vivo-compatible dyes and nanoprobes, the capacity for non-invasive cancer diagnosis and therapy will continue to advance significantly.

7. Two-Photon Imaging in Regenerative Science

Regenerative science is a frontier field in life sciences that investigates the potential of biological systems to self-repair and regenerate tissues and organs. Its core goal is to achieve functional restoration of damaged tissues and organs by activating or guiding cellular regenerative capacity. High spatiotemporal resolution in vivo imaging is a key approach for uncovering the underlying mechanisms of this process.

7.1. Stem Cell Imaging

Stem cells, often termed the body's "universal progenitor cells", possess dual capabilities: differentiating into specialized cells to replace aging or diseased tissues, and modulating immune responses to treat diseases. In vivo imaging of stem cells provides direct visualization of their differentiation and migration dynamics, revealing underlying disease mechanisms.

Two-photon SHG enables non-invasive monitoring of mesenchymal stem cells (MSCs) differentiation. Dynamic tracking of endogenous fluorophores—including NAD(P)H, flavoproteins, and lipofuscin—allows identification of metabolic activity changes through the redox ratio (calculated from the contributions of NAD(P)H and flavoproteins) across different culture media. Differentiation status is concurrently assessed via cell morphology from two-photon imaging and collagen synthesis detected by SHG [174]. Based on the fluorescence properties of NAD(P)H and FAD, two-photon FLIM could elucidate metabolic changes during adipogenic differentiation of MSCs. Analysis of protein-bound NAD(P)H lifetime contributions reveals a metabolic switch from glycolysis to OXPHOS in adipocytes [175]. Metabolic imaging of MSCs during osteogenic and chondrogenic differentiation shows that biosynthetic processes associated with the synthesis of collagen drive energy metabolism in differentiating cells and promote a metabolic shift from a more oxidative to a more glycolytic state [176].

TPM facilitates real-time and long-term observation of skin-resident stem cell activity within the intact skin of live mice, crucial for understanding skin homeostasis and wound healing [177]. It can also delineate how the compartmentalized organization of functionally diverse stem cell populations supports the maintenance and regeneration of an adult organ [178]. In vivo imaging tracks the migration, homing, proliferation, and differentiation of transplanted stem cells within host tissues [179]. Ex vivo two-photon imaging of muscle stem cells within their native niche environment enables detailed analysis of cell morphology, protrusion structures, and stem cell population dynamics at single-cell resolution [180].

7.2. Monitoring of Tissue Regeneration and Repair

TPM plays a crucial role in real-time monitoring of tissue regeneration and repair. For instance, the combination of TPM and SHG imaging allows for the assessment of the role of MSCs-seeded acellular dermal matrix in skin wound healing. It also enables the monitoring of changes in the collagen network during wound healing and the evaluation of the effects of different therapies [181]. Furthermore, this technique enables imaging of cardiomyocytes and collagen in healthy, infarcted, and stem cell-treated regenerating hearts, allowing for comparative analysis of the microstructural architecture of rat hearts under healthy, myocardial infarction, and stem cell therapy conditions. It provides a high-resolution, non-invasive visualization method for assessing the extent of myocardial damage, scar formation, and the therapeutic efficacy of stem cell-based cardiac repair [182]. In renal disease research, Zhang, K. et al. applied extracellular vesicles (EVs) derived from human placenta-derived mesenchymal stem cells (hP-MSCs) to a Sox9 transgenic mouse model of acute kidney injury (AKI). By establishing an abdominal imaging window and integrating two-photon imaging, the study achieved real-time tracing of $Sox9^+$ cells in the AKI mouse model. The results demonstrated that EVs could migrate specifically to the injured kidneys, promote proliferation and differentiation of $Sox9^+$ cells, participate in tubular epithelial regeneration, and significantly improve renal function. This approach provides a practical and visual strategy for investigating the role and underlying mechanisms of regenerative therapies in AKI [183]. Shen, B. et al. dissect the regenerative processes underlying structural recovery and cellular interplay across the entire visual pathway in larval zebrafish with an optic nerve transection model, using two-photon imaging and optokinetic response assays. This approach enabled high-resolution imaging of the entire visual pathway, capturing the dynamics of green fluorescent protein (GFP)-labeled retinal ganglion cell (RGC) axons, optic nerve projections, and tectal reinnervation following optic nerve transection. The study further confirmed that guidance from the contralateral eye is critical for functional regeneration of the optic nerve. This imaging framework provides a powerful tool for deciphering mechanisms of visual circuit reconstruction and identifying potential therapeutic targets for human optic neuropathies [184].

Tendon is a matrix-rich tissue with a limited number of cells. Owing to its high collagen abundance, the tendon serves as an ideal candidate for TPM analysis. TPM enables the imaging of cells in deep tissue layers and the characterization of extracellular matrix (ECM) architecture. In particular, collagen fibers and their orientation can be visualized via SHG signals, which is critical for elucidating the roles of stem cells in tendon repair and other tissue regeneration processes [185]. Mammalian tendons exhibit poor regenerative capacity and tend to form scar tissue during healing. In contrast, amphibian newts can achieve complete structural and functional regeneration after tendon transection. Kamiya T et al. established a two-photon imaging technique, which allows dynamic monitoring of the entire tendon regeneration process in individual newts at micro- and nanoscales. During regeneration, collagen fiber architecture gradually matures over time, accompanied by the restoration of mechanical properties. This study first uncovered the structural mechanisms underlying newt tendon transection regeneration, laying a fundamental foundation for exploring strategies to enhance tendon regenerative capacity in mammals [186]. In the field of bone repair, two-photon imaging permits the in situ observation and evaluation of the dynamic behaviors of osteoclasts in the bone marrow of live mice. This imaging modality can distinguish osteoclasts under inflammatory pathological conditions from those under physiological homeostasis and further clarify their differentiation mechanisms [187]. Furthermore, TPM is indispensable for investigating angiogenesis and its underlying molecular mechanisms. It possesses unique advantages in visualizing the deep 3D vascular architecture in various tissues, including both fixed specimens and the in vivo vasculature of

living organisms. This technique can resolve morphological and subcellular changes in cells and tissues during angiogenesis, providing high-quality imaging support for deciphering the molecular mechanisms of angiogenesis in regenerative medicine and biological research [188].

7.3. Organoids Imaging

Organoids are miniature and simplified organ models generated by the in vitro culture of stem cells or progenitor cells. They can recapitulate tissue-specific structures and execute physiological functions analogous to native organs, serving as powerful tools for investigating development, homeostasis, regeneration, and disease pathogenesis. And the imaging of organoids has become a pivotal method to visualize and understand their self-organization, symmetry breaking, growth, differentiation, and function [189].

Tomasi, S. et al. established an organoid model derived from human induced pluripotent stem cells that mimics the early human forebrain. By specifically labeling excitatory and inhibitory neuronal lineages, combined with TPM and CLARITY tissue clearing technology, they achieved whole-organoid 3D immunostaining, neuromorphological reconstruction, and quantitative analysis. This study deciphered the layered architecture, neural circuit connectivity, and inter-individual molecular and cellular heterogeneity of brain organoids [190]. Integration of transparent microelectrode arrays with two-photon imaging enables long-term multimodal monitoring of human cortical organoids transplanted into the mouse brain. Two-photon imaging validated robust organoid vascularization, as well as the formation of functional connections and synaptic integration between organoids and the host brain. This study established an in vivo platform for systematically evaluating the development, maturation, and neural circuit integration of human brain organoids [191]. To improve the quality control of organoids, Xue, Y. et al. introduced TPM to longitudinally monitor the developmental characteristics of retinal organoids (RtOgs) in a non-invasive manner. FLIM was applied to track metabolic profiles, and hyperspectral imaging was used to characterize structural and molecular alterations during development. Using this integrated imaging strategy, the metabolic transition patterns and photoreceptor maturation timeline during organoid differentiation were clarified. Meanwhile, the consistency of developmental profiles among different batches of organoids and the structural and cellular similarity to the native human retina were validated. These findings provide a reliable technical basis for long-term functional evaluation and standardized quality control of RtOgs [192].

In summary, the future of regenerative science relies on the capability to precisely regulate stem cells to generate functional tissues. Two-photon imaging allows the visualization and tracking of stem cell phenotypes, migration and differentiation, and enables the dissection of complex biological processes such as tissue regeneration and neural circuit dynamics, thereby facilitating standardized quality control of organoids. Continuous technological innovation and combinatorial application with other advanced imaging modalities are steadily expanding the research frontiers of regenerative science.

8. Two-Photon Imaging in Plants

Confocal microscopy is a powerful tool for biological imaging in plant sciences, but imaging deep plant tissues remains challenging due to intrinsic autofluorescence, high optical density of tissues, and multiply scattering structures that reduce image clarity [193]. TPM allows deep penetration into plant tissues and high-resolution 3D reconstruction, facilitating studies of plant cellular structures and functions, as shown in Figure 3.

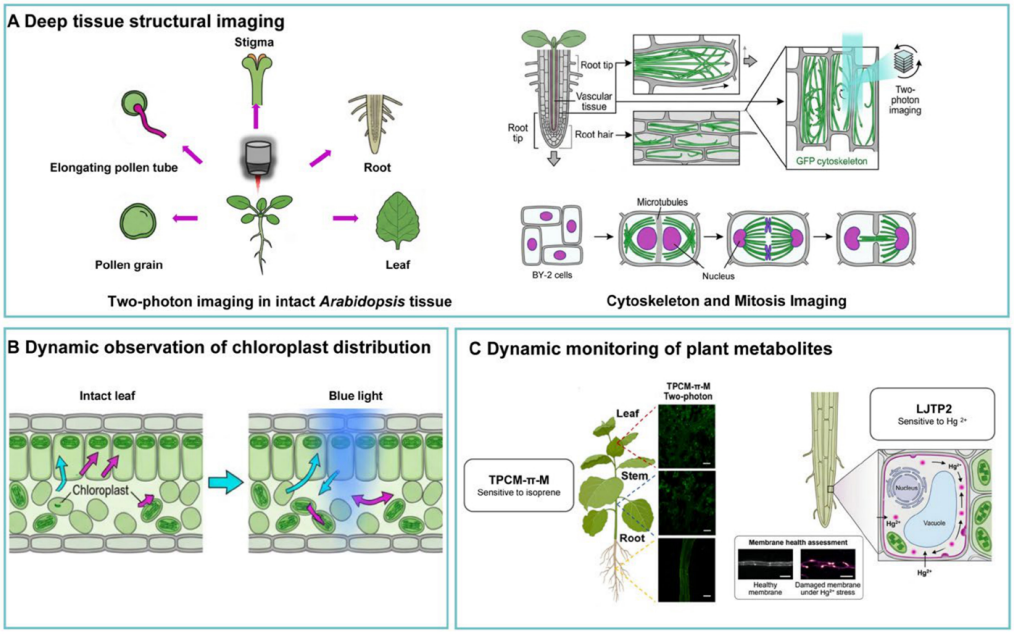

Figure 3. Two-photon imaging in plants: from structural imaging to dynamic organelle behavior and metabolite sensing. Copyright 2025, Elsevier [194].

8.1. Deep Imaging of Plant Tissue Structure

Tai S.P. et al. used a hollow photonic crystal fiber-based TPM to achieve two-photon fluorescence (chlorophyll) imaging of mesophyll tissue in leaves. With average power exposure below 2 mW at 755 nm—a wavelength near zero-dispersion—the distribution of chloroplasts within mesophyll cells could be resolved with sub-micrometer spatial resolution [195]. In 2015, Mizuta Y. demonstrated the advantages of TPM for deep imaging in live, intact Arabidopsis thaliana tissues. Compared to single-photon imaging, TPM using near-infrared wavelengths—particularly at 1000 nm—significantly reduced chloroplast autofluorescence; decreased autofluorescence was also observed in leaves, roots, stigmas, and pollen grains. Additionally, TPM at 980 nm enabled multicolor imaging of Arabidopsis pollen tubes through simultaneous excitation [196]. Two-photon FLIM is also used to analyze the distribution and characteristics of Photosystem I (PSI) and Photosystem II (PSII) in palisade and spongy chloroplasts of C3 plant Arabidopsis thaliana and C4 plant Miscanthus x giganteus leaves. Studies reveal that in Arabidopsis, the PSII antenna size is larger on the abaxial side of the leaf due to spongy mesophyll chloroplasts being shaded by palisade cells. Additionally, PSI contains slightly more chlorophyll on the adaxial side of the leaf. In the C4 plant M. x giganteus, mesophyll and bundle sheath cells exhibit distinct PSI/PSII ratios [197]. Zhang N. et al. utilized TPM to study Arabidopsis thaliana seedlings, comparing the staining patterns of three phthalocyanine derivatives in roots and leaves. The study revealed subtle structural differences among the derivatives and further demonstrated deep tissue penetration and high-resolution 3D reconstruction in plant tissues, establishing a new application paradigm for novel near-infrared two-photon fluorescent compounds in live plant imaging [198]. Stefanie R. et al. used two-photon photoactivation to measure histone exchange dynamics in plant root cells, providing a new method to study the role of chromatin-associated proteins in chromatin structure and gene expression [199].

The cytoskeleton plays a crucial role in plant cells during processes such as development and morphological changes. Wang P. F et al. from Tsinghua University used TPM, suitable for live four-dimensional imaging of large and thick samples, to observe cytoskeletal structures within root tips, vessels, and root hairs of live-transfected GFP-Arabidopsis

seeds, as well as the dynamic growth and development of Arabidopsis root tips [200]. Plant cells exhibit unique microtubule organization during mitosis. However, observing cell division in plant cells is challenging due to image distortion caused by thick samples. Takashi M. et al. developed a method to visualize microtubules and nuclei during cell division in tobacco BY-2 cells using two-photon spinning-disk confocal microscopy [201].

In 2024, Safaee M. M. et al. developed a groundbreaking dual-infrared TPM (Dual-IR 2PM), pushing both excitation and emission wavelengths into the NIR-II window, using single-walled carbon nanotubes (SWCNTs) as fluorophores. In imaging tobacco leaf tissues, the system achieved full-depth imaging across the entire 120 μm thickness with extremely low autofluorescence background [202]. In 2025, Chen Z. introduced two-photon FLIM into maize C_4 photosynthesis research, achieving the first direct resolution of photosynthetic characteristics in bundle sheath cells under live conditions. C_4 plants achieve efficient photosynthesis through metabolic compartmentalization between mesophyll and bundle sheath cells, but ex vivo measurements often disrupt this delicate anatomical structure, leading to abnormal photosynthetic activity. Two-photon FLIM provides a non-invasive, in situ observation window, enabling researchers to directly measure photosynthetic parameters in different cell types within intact leaves [203]. In addition, Stoneman M.R. et al. applied two-photon fluorescence spectroscopy to the fluorescence characterization of fossil plants. They resolved fluorescence emitted from amber-encased plants, leaf compressions, and silicified wood, observing potential signals from chlorophyll derivatives/tannins, opening doors to exploring ancient ecosystems and understanding the ecological roles of plants throughout evolutionary history [204]. This work extends the application of two-photon imaging from live biological systems to paleobotany, where its pixel-level spectral resolution and line-scan excitation strategy enable rich fluorescence data acquisition while minimizing laser-induced damage to precious specimens.

8.2. Chloroplast Spatial Distribution Dynamics Observation

Chloroplast spatial distribution dynamics are crucial for optimizing photosynthetic capacity under fluctuating light conditions. Light-induced chloroplast movement has been widely studied, but most research has been conducted on isolated tissues or protoplasts. Ryu J. et al. employed TPM to monitor 3D intracellular chloroplast movement in intact plant leaves during the transition from dark to light. In subepidermal mesophyll cells, chloroplasts typically move away from the surface after blue light exposure, yet many chloroplasts show no movement. This spatial heterogeneity in chloroplast motility highlights the importance of monitoring intracellular orientation and movement of individual chloroplasts within intact leaves [205]. Plant chloroplasts perform photosynthesis, converting solar energy into sugars—the essential carbon source for cellular life and growth during the day. A portion of the photosynthetic products is stored within chloroplasts as starch granules, which sustain the carbon energy supply at night. Liao J.N. et al. used two-photon fluorescence imaging to quantify starch granules in chloroplasts of fresh, intact leaves across the diurnal cycle [206]. Additionally, two-photon FLIM enables rapid, non-invasive assessment of cadmium (Cd)-induced toxicity in marine diatoms. Chlorophyll fluorescence lifetime images collected from diatom samples exposed to varying Cd concentrations clearly revealed structural changes in chloroplasts under higher Cd levels [207].

8.3. Dynamic Monitoring of Plant Metabolites

In recent years, two-photon imaging has rapidly advanced in the real-time tracking of spatiotemporal dynamics of specific metabolites within deep living plant tissues. Isoprene plays a dual role in plant stress protection and air pollution, yet its insufficient spatiotemporal monitoring in plants has limited environmental risk assessment. In 2025, Su

C. et al. designed a fluorescent probe TPCM-π-M with excellent two-photon properties by systematically studying the effects of alkyne, maleimide groups, and conjugated structures on probe performance. The probe achieved a linear response to isoprene over a range of 1–240 ppm with a detection limit as low as 0.2 ppm. Using two-photon imaging, the study resolved the spatial distribution of endogenous isoprene in deep plant tissues, overcoming the limited penetration depth of traditional single-photon imaging. It enabled dynamic visualization of isoprene metabolism under abiotic stress, revealing the metabolic regulation mechanism under a carotenoid/photorespiration inhibition mode [194]. Mercury ions (Hg^{2+}) cause severe stress in plants by disrupting cell cycle progression, photosynthesis, and ion homeostasis. Accurate visualization of their spatiotemporal distribution in plant tissues is critical for mercury pollution mitigation. Also in 2025, a research journal reported a highly sensitive fluorescent probe LJTP2, capable of detecting Hg^{2+} with high specificity and sensitivity (~16 nM) at the subcellular level. Leveraging two-photon fluorescence imaging with this probe, researchers not only visualized the dynamic distribution of Hg^{2+} within plant cells but also assessed cell membrane health status under Hg^{2+} stress. This provides a crucial imaging tool for elucidating the molecular mechanisms of Hg^{2+} stress in plants, highlighting the application potential of small-molecule fluorescent probes in plant science [208].

In two-photon fluorescence imaging of plant tissues, intrinsic autofluorescence is a double-edged sword. On one hand, plant tissues are rich in strong endogenous fluorophores such as chlorophyll, carotenoids, lignin, and phenolic compounds, which enable label-free imaging using TPM. On the other hand, these molecules are also the primary source of background noise, severely interfering with the detection of the exogenous fluorescence signal [209]. Although the dual-infrared TPM reported by Safaee et al. in 2024 achieved full-depth imaging in leaf tissue with "extremely low autofluorescence background [202], this approach currently relies on exogenous nanomaterial labeling and has not yet resolved the spectral separation challenge when using endogenous fluorescence for functional imaging. Moreover, compared to the fields of neurobiology and immunology, two-photon fluorescent probes specifically designed for the chemical environment of living plants are extremely scarce. Two-photon-specific probes for key signaling molecules and metabolites in plants—such as auxin, jasmonic acid, ROS, and calcium dynamics—remain severely lacking. The development of novel fluorescent probes has thus become one of the core driving forces advancing live-cell imaging in plants.

9. Prospects

Since its invention, TPM has rapidly advanced across multiple dimensions, as shown in Figure 4. However, complex biological processes occur across wide temporal and spatial scales, often limiting comprehensive investigations. TPM still exhibits certain shortcomings and limitations in temporal resolution, large-scale network monitoring, long-term applicability, and recording neural activity in freely moving animals behaving naturally. Current advancements in TPM imaging technology are accelerating around several core directions, aiming to overcome the limitations of traditional techniques and expand new research frontiers. This progress is mainly concentrated in the following four aspects.

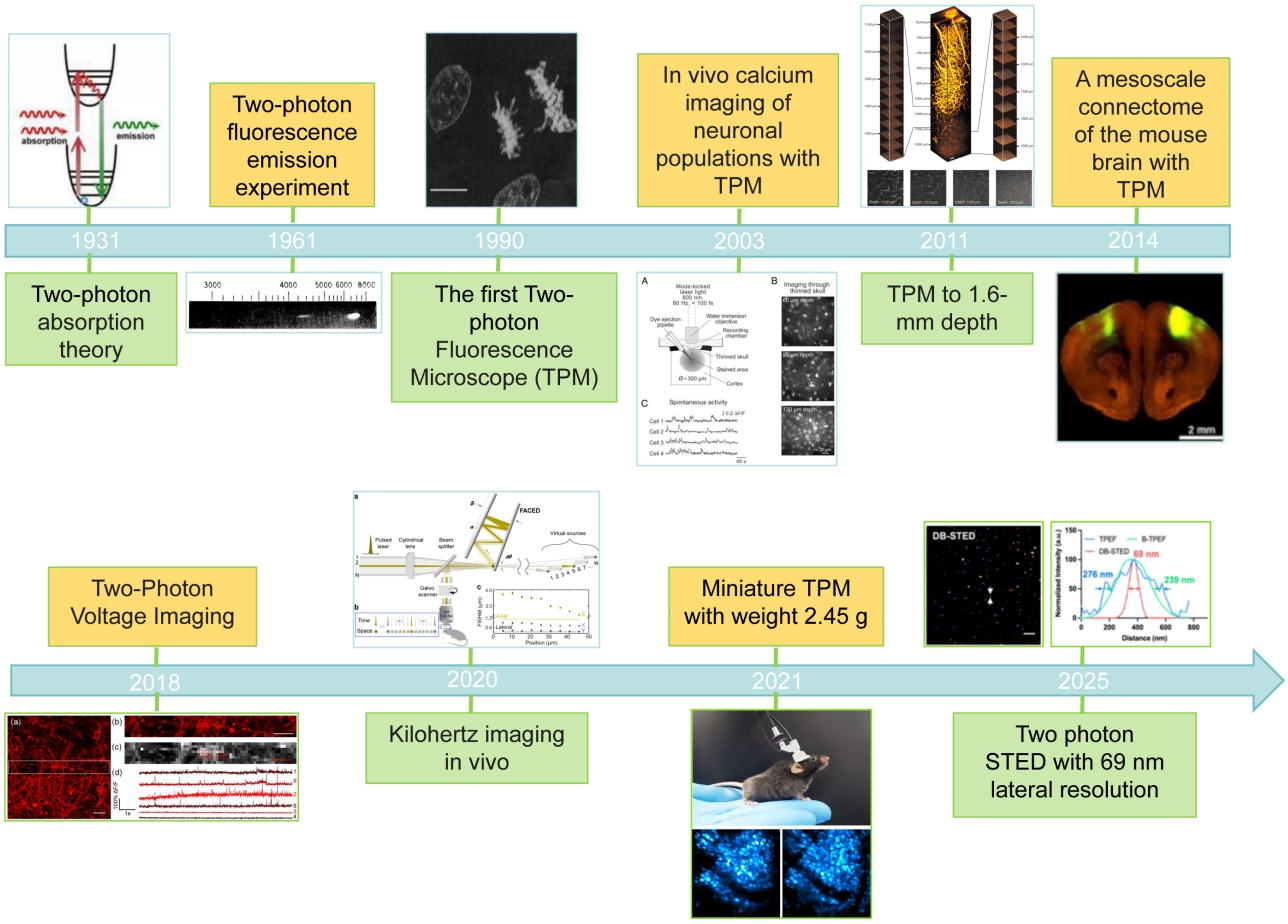

Figure 4. The Progress of TPM development and its applications. Copyright 1961, American Physical Society [2]. Copyright 1990, American Association for the Advancement of Science [3]. Copyright 2003, National Academy of Sciences [65]. Copyright 2011, The International Society for Optics and Photonics [9]. Copyright 2014, Springer Nature [210]. Copyright 2018, American Chemical Society [211]. Copyright 2020, Springer Nature [6]. Copyright 2021, Springer Nature [12]. Copyright 2025, American Chemical Society [74].

First, enhanced large FOV and deep tissue imaging. Large FOV and deep tissue imaging enable holistic observation of large-scale neural networks or organ tissues, facilitating research into the macroscopic functions of biological systems. The design of the multi-area two-photon real-time in vivo explorer (MATRIEX) enables the imaging of multiple functional brain regions distributed within a zone of up to 12 mm in diameter, each with a FOV of 200 μm in diameter [212]. Using 1280 nm excitation, a record imaging depth of 1.6 mm in the mouse cortex can be achieved in vivo [9]. Simultaneously, the development of high-performance two-photon fluorescent probes [213,214] focuses on optimizing molecular structure design to synergistically enhance probe penetration capability, fluorescence signal intensity, and fluorescence lifetime, thereby enabling effective imaging of deeper tissue layers.

Second, breakthroughs in high-resolution imaging. The diffraction limit remains the primary constraint on the resolution of optical microscopes. Research on biomolecular interactions and detailed characterization of subcellular structures urgently demands nanoscale resolution. Structured illumination technology enables breakthroughs beyond the diffraction limit by spatially mixing high-frequency object information into the detection bandwidth of optical systems in the frequency domain, thereby achieving higher-resolution [215]. Furthermore, integrating STED super-resolution technology [216] with TPM can further

enhance spatial resolution to 69 nm [13], enabling nanoscale imaging capabilities. These technologies provide powerful tools for investigating the mechanisms of subcellular-level biological activities.

Third, optimization of imaging speed. Core biological processes such as neuronal electrical activity and cellular signaling exhibit millisecond-scale dynamics. The imaging speed of traditional TPM (typically ranging from hertz to tens of hertz) struggles to capture these transient events. With the advent of random-scan microscopy, laser beams can now move within microseconds, enabling imaging speeds to reach the kilohertz range and achieving true high-speed random-access imaging [217,218]. Furthermore, multi-beam scanning technology simultaneously excites multiple imaging points, significantly enhancing scanning efficiency and further pushing the upper limits of imaging speed [219].

Fourth, functional integration and diversification. Biological information obtained through single imaging techniques has inherent limitations. Integrating TPM with complementary imaging technologies to construct multimodal imaging systems has become a core trend for enhancing biological information dimensionality. For instance, combining TPM with Raman spectroscopy [220], photoacoustic imaging [221], and fluorescence lifetime imaging [222] enables simultaneous acquisition of multidimensional information—including structural features, chemical composition, and metabolic activity. Furthermore, integrating TPM with optogenetics [223] and optical tweezers [224] enables optical manipulation capabilities, providing powerful tools for precise control and in-depth investigation of biological processes.

Although TPM has made remarkable progress, it is critical to recognize that current techniques have achieved significant breakthroughs in only one or two of the key parameters—FOV, resolution, imaging depth, speed, and miniaturization. This limitation stems from the formidable technical barrier of synergistically optimizing multiple interdependent parameters. Existing strategies primarily refine or balance individual parameters, unable to concurrently enhance all dimensions. Future efforts should pursue novel optical architectures that enable universal, cost-effective multi-dimensional optimization. Such innovations could overcome the current trade-offs and expand the applicability of TPM in complex, live biological systems.

10. Conclusions

Since its introduction in 1990, TPM has evolved from a proof-of-concept technique into an indispensable in vivo imaging platform in life sciences. Its core advantages stem from the physical nature of nonlinear optical effects—using near-infrared femtosecond pulsed lasers to achieve two-photon excitation of fluorescent molecules, restricting fluorescence emission strictly within a tiny volume at the focal point of the objective. This mechanism provides three fundamental benefits: inherent optical sectioning enables high-contrast 3D imaging without the need for a confocal pinhole; the deep tissue penetration of near-infrared excitation extends imaging depth from approximately 100 micrometers in confocal microscopy to hundreds of micrometers or even millimeters; and focal-restricted excitation significantly reduces phototoxicity and photobleaching, making long-term in vivo observations over hours or even days possible.

On the technological front, TPM has undergone multiple transformations—from benchtop systems to miniaturized devices, from monochromatic imaging to multicolor synchronous observation, and from structural recording to functional decoding. In terms of applications, beyond neuroscience, immunology, oncology, regenerative science and plants mentioned in this article, the technique has deeply penetrated key fields such as developmental biology, ophthalmology and vision science. Currently, TPM stands on the brink of a new wave of breakthroughs. The tight integration of super-resolution techniques

is pushing lateral resolution below 100 nanometers, promising nanoscale-resolution imaging in deep tissues. Multimodal integration is becoming increasingly prominent, with simultaneous acquisition of FLIM, SHG, and coherent Raman scattering enabling unified access to structural, functional, and molecular information. The deep integration of artificial intelligence is reshaping the entire imaging pipeline—from deep learning-based real-time image denoising and super-resolution reconstruction to automated sample targeting and intelligent focusing—continuously lowering technical barriers while enhancing image quality and throughput. As related technologies mature and gain widespread adoption, TPM will undoubtedly remain at the forefront of biological imaging trends, offering unprecedented perspectives for unraveling the essence of life.

Author Contributions: Q.B., conceptualization, writing, visualization, and investigation. Y.G., writing, editing and data curation. X.W., writing—review and editing and validation. S.Y., writing—review and editing. K.S., supervision, funding acquisition, and writing—review and editing. X.Z., supervision, funding acquisition, and writing—review and editing. All authors have read and agreed to the published version of the manuscript.

Funding: This research was funded by National Natural Science Foundation of China, grant number 62475258, and Natural Science Foundation of Changchun Normal University, grant number CSJJ2025008ZK.

Data Availability Statement: No new data were created or analyzed in this study. Data sharing is not applicable to this article.

Acknowledgments: During the preparation of this manuscript, the authors used Grammarly (1.2.211.1787) for the purpose of English editing. The authors have reviewed and edited the output and take full responsibility for the content of this publication.

Conflicts of Interest: The authors declare no conflicts of interest.

Abbreviations

The following abbreviations are used in this manuscript:

TPM	Two-photon microscopy
3D	Three-dimensional
EOM	Electro-optical modulator
AOM	Acousto-optic modulator
SG	Scanning galvanometer
DM	Dichroic mirror
PMT	Photomultiplier tube
2D	Two-dimensional
SNR	Signal-to-Noise Ratio
SRRF	Super-resolution radial fluctuation
SIM	Structured illumination microscopy
STED	Stimulated emission depletion
AO	Adaptive optics
FLIM	Fluorescence lifetime imaging microscopy
SHG	Second harmonic generation
ROS	Reactive oxygen species
EVs	Extracellular vesicles
PKM2	Pyruvate kinase M2
OXPHOS	Oxidative phosphorylation
AE	Affective empathy
ULTRA	Ultra-wide, Layer-penetrating, Two-photon, Responsive Adaptive microscope
FOV	Field of view

PEO-CYTOP	Polyethylene-oxide-coated CYTOP
AD	Alzheimer's disease
PD	Parkinson's disease
MPTP	1-Methyl-4-phenyl-1,2,3,6-tetrahydropyridine
MHC	Major histocompatibility complex
FAD	Flavin adenine dinucleotide
NAD(P)H	Nicotinamide adenine dinucleotide
EAE	Experimental autoimmune encephalomyelitis
Tregs	Regulatory T cells
DCs	Dendritic cells
HBV	Hepatitis B virus
GC	Germinal centers
MΦs	Macrophages
MIF	Migration inhibitory factor
G-CSF	Granulocyte colony-stimulating factor
VLA-4	Very-late-antigen-4
SCT-TPM	Supercontinuum-truncated two-photon microscopy
CAR-T	Chimeric antigen receptor T-cell
CTL	Cytotoxic T lymphocyte
PDA	Polydopamine
OPDA	Oxidized polydopamine
aPD-1	Monoclonal antibodies targeting the immune checkpoint PD-1
TPSS	Two-photon photosensitizer
CA IX	Carbonic anhydrase IX
H&E	Hematoxylin and eosin
N-BN	Unique red-emitting two-photon probe
NTR	Nitroreductase
CSCs	Cancer stem cells
NIR-II	Near-infrared II
NQO1	Quinone oxidoreductase 1
GSH	Glutathione
HClO	Hypochlorous acid
LD	Lipid droplet
Trp	Tryptopha
RGD	L-arginine (R), glycine (G), and L-aspartic acid (D) residues
LLC	Lewis lung carcinoma
AIE	Aggregation-induced emission
TAM/M	Tumor-associated macrophages/microglia
PDT	Photodynamic therapy
TP-PDT	Two-photon photodynamic therapy
MPPa	Pyropheophorbide-α methyl ester
AlPcS	Sulfonated aluminum phthalocyanine
TPAs	Triphenylamines
TCS	TiO_2-CUR-Sofast
CUR	Curcumin
MSCs	Mesenchymal stem cells
EVs	Vesicles
hP-MSCs	Mesenchymal stem cells
AKI	Acute kidney injury
GFP	Green fluorescent protein
RGC	Retinal ganglion cell
ECM	Extracellular matrix
RtOgs	Retinal organoids
PSI	Photosystem I

PSII	Photosystem II
Dual-IR 2PM	Dual-infrared TPM
SWCNTs	Single-walled carbon nanotubes
MATRIEX	Multiarea two-photon real-time in vivo explorer

References

1. Göppert-Mayer, M. Über Elementarakte mit zwei Quantensprüngen. *Ann. Phys.* **1931**, *401*, 273–294.
2. Kaiser, W.; Garrett, C.G.B. Two-photon excitation in CaF_2: Eu^{2+}. *Phys. Rev. Lett.* **1961**, *7*, 229–231. [CrossRef]
3. Denk, W.; Strickler, J.H.; Webb, W.W. Two-photon laser scanning fluorescence microscopy. *Science* **1990**, *248*, 73–76. [CrossRef]
4. Sofroniew, N.J.; Flickinger, D.; King, J.; Svoboda, K. A large field of view two-photon mesoscope with subcellular resolution for in vivo imaging. *eLife* **2016**, *5*, e14472. [PubMed]
5. Meng, G.; Liang, Y.; Sarsfield, S.; Jiang, W.C.; Lu, R.; Dudman, J.T.; Aponte, Y.; Ji, N. High-throughput synapse-resolving two-photon fluorescence microendoscopy for deep-brain volumetric imaging in vivo. *eLife* **2019**, *8*, e40805. [CrossRef] [PubMed]
6. Wu, J.; Liang, Y.; Chen, S.; Hsu, C.L.; Chavarha, M.; Evans, S.W.; Shi, D.; Lin, M.Z.; Tsia, K.K.; Ji, N. Kilohertz two-photon fluorescence microscopy imaging of neural activity in vivo. *Nat. Methods* **2020**, *17*, 287–290. [CrossRef] [PubMed]
7. Xu, C.; Zipfel, W.; Shear, J.B.; Williams, R.M.; Webb, W.W. Multiphoton fluorescence excitation: New spectral windows for biological nonlinear microscopy. *Proc. Natl. Acad. Sci. USA* **1996**, *93*, 10763–10768.
8. Cox, G.; Sheppard, C.J. Practical limits of resolution in confocal and non-linear microscopy. *Microsc. Res. Tech.* **2004**, *63*, 18–22.
9. Kobat, D.; Horton, N.G.; Xu, C. In vivo two-photon microscopy to 1.6-mm depth in mouse cortex. *J. Biomed. Opt.* **2011**, *16*, 106014. [CrossRef]
10. Helmchen, F.; Denk, W. Deep tissue two-photon microscopy. *Nat. Methods* **2005**, *2*, 932–940. [CrossRef]
11. Tsutsumi, M.; Takahashi, T.; Kobayashi, K.; Nemoto, T. Fluorescence radial fluctuation enables two-photon super-resolution microscopy. *Front. Cell. Neurosci.* **2023**, *17*, 1243633. [CrossRef]
12. Wang, L.; Zheng, X.; Zhou, J.; Wang, M.; Chen, J.; Zeng, Y.; Xu, G.; Wang, Y.; Qiu, H.; Shao, Y.; et al. Improvement in Resolution of Multiphoton Scanning Structured Illumination Microscopy via Harmonics. *Engineering* **2022**, *16*, 65–72. [CrossRef]
13. Zhang, R.; Zhou, H.; Wang, C.; Weng, X.; Liu, L.; Xi, P.; Qu, J. Dual-Bessel-Beam Stimulated Emission Depletion Microscopy for Super-resolution Volumetric Projection Imaging of Lipid Droplet Dynamics. *Nano Lett.* **2025**, *25*, 5557–5564. [CrossRef] [PubMed]
14. Yoshioka, M.; Takahashi, M.; Kershaw, J.; Handa, M.; Takada, A.; Takuwa, H. Two-photon optogenetics-based assessment of neuronal connectivity in healthy and chronic hypoperfusion mice. *Neurophotonics* **2024**, *11*, 035009. [CrossRef] [PubMed]
15. Yao, J.; Gao, Y.; Yin, Y.; Lai, P.; Ye, S.; Zheng, W. Exploiting the potential of commercial objectives to extend the field of view of two-photon microscopy by adaptive optics. *Opt. Lett.* **2022**, *47*, 989–992. [CrossRef]
16. Yao, P.; Liu, R.; Broggini, T.; Thunemann, M.; Kleinfeld, D. Construction and use of an adaptive optics two-photon microscope with direct wavefront sensing. *Nat. Protoc.* **2023**, *18*, 3732–3766. [CrossRef]
17. Hu, Q.; Wang, J.; Antonello, J.; Hailstone, M.; Wincott, M.; Turcotte, R.; Gala, D.; Booth, M. A universal framework for microscope sensorless adaptive optics: Generalized aberration representations. *APL Photonics* **2020**, *5*, 100801. [CrossRef]
18. Shcheslavskiy, V.I.; Shirmanova, M.V.; Yashin, K.S.; Ruck, A.C.; Skala, M.C.; Becker, W. Fluorescence Lifetime Imaging Techniques—A Review on Principles. Applications and Clinical Relevance. *J. Biophotonics* **2025**, *18*, e202400450. [CrossRef]
19. Shirshin, E.A.; Shirmanova, M.V.; Gayer, A.V.; Lukina, M.M.; Nikonova, E.E.; Yakimov, B.P.; Budylin, G.S.; Dudenkova, V.V.; Ignatova, N.I.; Komarov, D.V.; et al. Label-free sensing of cells with fluorescence lifetime imaging: The quest for metabolic heterogeneity. *Proc. Natl. Acad. Sci. USA* **2022**, *119*, e2118241119. [CrossRef] [PubMed]
20. Yaseen, M.A.; Sakadzic, S.; Wu, W.; Becker, W.; Kasischke, K.A.; Boas, D.A. In vivo imaging of cerebral energy metabolism with two-photon fluorescence lifetime microscopy of NADH. *Biomed. Opt. Express* **2013**, *4*, 307–321. [CrossRef]
21. Feeks, J.A.; Hunter, J.J. Adaptive optics two-photon excited fluorescence lifetime imaging ophthalmoscopy of exogenous fluorophores in mice. *Biomed. Opt. Express* **2017**, *8*, 2483–2495. [CrossRef]
22. Hanson, K.M.; Behne, M.J.; Barry, N.P.; Mauro, T.M.; Gratton, E.; Clegg, R.M. Two-photon fluorescence lifetime imaging of the skin stratum corneum pH gradient. *Biophys. J.* **2002**, *83*, 1682–1690. [CrossRef]
23. Lazzari-Dean, J.R.; Miller, E.W. Optical Estimation of Absolute Membrane Potential Using One- and Two-Photon Fluorescence Lifetime Imaging Microscopy. *Bioelectricity* **2021**, *3*, 197–203. [CrossRef] [PubMed]
24. Halip, H.; Yoshimura, Y.; Inami, W.; Kawata, Y. Ultrashort laser based two-photon phase-resolved fluorescence lifetime measurement method. *Methods Appl. Fluoresc.* **2020**, *8*, 025003. [CrossRef] [PubMed]
25. Lahn, M.; Dosche, C.; Hille, C. Two-photon microscopy and fluorescence lifetime imaging reveal stimulus-induced intracellular Na^+ and Cl^- changes in cockroach salivary acinar cells. *Am. J. Physiol. Cell Physiol.* **2011**, *300*, C1323–C1336. [CrossRef]
26. Chen, S.; Hong, Y.; Zeng, Y.; Sun, Q.; Liu, Y.; Zhao, E.; Bai, G.; Qu, J.; Hao, J.; Tang, B.Z. Mapping live cell viscosity with an aggregation-induced emission fluorogen by means of two-photon fluorescence lifetime imaging. *Chemistry* **2015**, *21*, 4315–4320. [CrossRef] [PubMed]

27. Yeh, A.T.; Nassif, N.; Zoumi, A.; Tromberg, B.J. Selective corneal imaging using combined second-harmonic generation and two-photon excited fluorescence. *Opt. Lett.* **2002**, *27*, 2082–2084. [CrossRef]
28. Sun, Y.; Li, L.; Ma, S.; He, G.; Yang, W.; Wang, Y. In vivo Visualization of Collagen Transdermal Absorption by Second-Harmonic Generation and Two-Photon Excited Fluorescence Microscopy. *Front. Chem.* **2022**, *10*, 925931. [CrossRef]
29. Bueno, J.M.; Martinez-Ojeda, R.M.; Perez-Zabalza, M.; Garcia-Mendivil, L.; Asensio, M.C.; Ordovas, L.; Pueyo, E. Analysis of age-related changes in the left ventricular myocardium with multiphoton microscopy. *Biomed. Opt. Express* **2024**, *15*, 3251–3264. [CrossRef]
30. Bell, J.S.; Adio, A.O.; Pitt, A.; Hayman, L.; Thorn, C.E.; Shore, A.C.; Whatmore, J.L.; Winlove, C.P. Microstructural Characterization of Resistance Artery Remodelling in Diabetes Mellitus. *J. Vasc. Res.* **2022**, *59*, 50–60. [CrossRef]
31. Ren, W.; Guo, W.; Kang, D.; Han, Z.; He, J.; Xi, G.; Wang, C.; Chen, J.; Li, L. Visualization of lymphatic vascular invasion in breast cancer by multiphoton microscopy. *Lasers Med. Sci.* **2021**, *36*, 303–309. [CrossRef] [PubMed]
32. Xie, X.S. 25 years of 3D coherent Raman imaging for biomedicine. *Nat. Methods* **2025**, *22*, 877–882. [CrossRef]
33. Hou, J.; Williams, J.; Botvinick, E.L.; Potma, E.O.; Tromberg, B.J. Visualization of Breast Cancer Metabolism Using Multimodal Nonlinear Optical Microscopy of Cellular Lipids and Redox State. *Cancer Res.* **2018**, *78*, 2503–2512. [CrossRef]
34. Calvarese, M.; Corbetta, E.; Contreras, J.; Bae, H.; Lai, C.; Reichwald, K.; Meyer-Zedler, T.; Pertzborn, D.; Muhlig, A.; Hoffmann, F.; et al. Endomicroscopic AI-driven morphochemical imaging and fs-laser ablation for selective tumor identification and selective tissue removal. *Sci. Adv.* **2024**, *10*, eado9721. [CrossRef]
35. Schmitt, P.D. Recent Advances in Nonlinear Optical Analyses of Pharmaceutical Materials in the Solid State. *Mol. Pharm.* **2017**, *14*, 555–565. [CrossRef]
36. Kucikas, V.; Werner, M.P.; Schmitz-Rode, T.; Louradour, F.; van Zandvoort, M. Two-Photon Endoscopy: State of the Art and Perspectives. *Mol. Imaging Biol.* **2023**, *25*, 3–17. [CrossRef]
37. Ducourthial, G.; Leclerc, P.; Mansuryan, T.; Fabert, M.; Brevier, J.; Habert, R.; Braud, F.; Batrin, R.; Vever-Bizet, C.; Bourg-Heckly, G.; et al. Development of a real-time flexible multiphoton microendoscope for label-free imaging in a live animal. *Sci. Rep.* **2015**, *5*, 18303. [CrossRef]
38. Liang, W.; Hall, G.; Messerschmidt, B.; Li, M.J.; Li, X. Nonlinear optical endomicroscopy for label-free functional histology in vivo. *Light Sci. Appl.* **2017**, *6*, e17082. [CrossRef]
39. Soleimany, A.; Aghmiouni, D.K.; Amirikhah, M.; Shokrgozar, M.A.; Khoee, S.; Sarmento, B. Two-Photon Mediated Cancer Therapy: A Comprehensive Review on Two-Photon Photodynamic Therapy and Two-Photon-Activated Therapeutic Delivery Systems. *Adv. Funct. Mater.* **2024**, *34*, 2408594. [CrossRef]
40. Marazzini, M.; Scalera, E.; De Meo, S.; Ricci, F.; Villetti, G.; Murgia, X.; Zoboli, M.; Gazza, F.; Ferri, G.; Cardarelli, F. Label-free optical fingerprints of hyperoxia-induced lung alterations in preterm rabbits. *Respir. Res.* **2026**, *27*, 153. [CrossRef] [PubMed]
41. Quansah, E.; Gardey, E.; Ramoji, A.; Meyer-Zedler, T.; Goehrig, B.; Heutelbeck, A.; Hoeppener, S.; Schmitt, M.; Waldner, M.; Stallmach, A. Intestinal epithelial barrier integrity investigated by label-free techniques in ulcerative colitis patients. *Sci. Rep.* **2023**, *13*, 2681. [CrossRef]
42. Svoboda, K.; Denk, W.; Kleinfeld, D.; Tank, D.W. In vivo dendritic calcium dynamics in neocortical pyramidal neurons. *Nature* **1997**, *385*, 161–165. [CrossRef] [PubMed]
43. Mostany, R.; Chowdhury, T.G.; Johnston, D.G.; Portonovo, S.A.; Carmichael, S.T.; Portera-Cailliau, C. Local hemodynamics dictate long-term dendritic plasticity in peri-infarct cortex. *J. Neurosci.* **2010**, *30*, 14116–14126. [CrossRef]
44. Grewe, B.F.; Langer, D.; Kasper, H.; Kampa, B.M.; Helmchen, F. High-speed in vivo calcium imaging reveals neuronal network activity with near-millisecond precision. *Nat. Methods* **2010**, *7*, 399–405. [CrossRef] [PubMed]
45. Takechi, H.; Eilers, J.; Konnerth, A. A new class of synaptic response involving calcium release in dendritic spines. *Nature* **1998**, *396*, 757–760. [CrossRef]
46. Sorrells, J.E.; Martin, E.M.; Aksamitiene, E.; Mukherjee, P.; Alex, A.; Chaney, E.J.; Marjanovic, M.; Boppart, S.A. Label-free characterization of single extracellular vesicles using two-photon fluorescence lifetime imaging microscopy of NAD(P)H. *Sci. Rep.* **2021**, *11*, 3308. [CrossRef]
47. Hefendehl, J.K.; LeDue, J.; Ko, R.W.; Mahler, J.; Murphy, T.H.; MacVicar, B.A. Mapping synaptic glutamate transporter dysfunction in vivo to regions surrounding Abeta plaques by iGluSnFR two-photon imaging. *Nat. Commun.* **2016**, *7*, 13441. [CrossRef]
48. Meng, G.; Zhang, Q.; Ji, N. High-Speed Neural Imaging with Synaptic Resolution: Bessel Focus Scanning Two-Photon Microscopy and Optical-Sectioning Widefield Microscopy. *Neuromethods* **2023**, *191*, 293–329.
49. Pan, F.; Gan, W.B. Two-photon imaging of dendritic spine development in the mouse cortex. *Dev. Neurobiol.* **2008**, *68*, 771–778. [CrossRef]
50. Gray, N.W.; Weimer, R.M.; Bureau, I.; Svoboda, K. Rapid redistribution of synaptic PSD-95 in the neocortex in vivo. *PLoS Biol.* **2006**, *4*, e370. [CrossRef] [PubMed]
51. Nimmerjahn, A.; Kirchhoff, F.; Helmchen, F. Resting microglial cells are highly dynamic surveillants of brain parenchyma in vivo. *Science* **2005**, *308*, 1314–1318. [CrossRef]

52. Kim, S.K.; Eto, K.; Nabekura, J. Synaptic structure and function in the mouse somatosensory cortex during chronic pain: In vivo two-photon imaging. *Neural Plast.* **2012**, *2012*, 640259. [CrossRef] [PubMed]
53. Durst, C.D.; Oertner, T.G. Imaging Synaptic Glutamate Release with Two-Photon Microscopy in Organotypic Slice Cultures. *Methods Mol. Biol.* **2022**, *2417*, 205–219. [PubMed]
54. Wei, Y.; Miao, Q.; Zhang, Q.; Mao, S.; Li, M.; Xu, X.; Xia, X.; Wei, K.; Fan, Y.; Zheng, X.; et al. Aerobic glycolysis is the predominant means of glucose metabolism in neuronal somata. which protects against oxidative damage. *Nat. Neurosci.* **2023**, *26*, 2081–2089. [CrossRef] [PubMed]
55. Peng, S.; Yang, X.; Meng, S.; Liu, F.; Lv, Y.; Yang, H.; Kong, Y.; Xie, W.; Li, M. Dual circuits originating from the ventral hippocampus independently facilitate affective empathy. *Cell Rep.* **2024**, *43*, 114277. [CrossRef]
56. Yang, M.; Zhou, Z.Q.; Lang, S.; Zheng, H.; Chen, S.; Li, T.; Stas, E.; Yu, J.; Zhang, L.; Zhang, Z.; et al. Ultra-wide-field. deep, adaptive two-photon microscopy for multi-scale neuronal imaging. *Light Sci. Appl.* **2026**, *15*, 198. [CrossRef]
57. Takahashi, T.; Makino, Y.; Okamura, Y.; Nemoto, T. Construction of Large Cranial Windows with Nanosheet and Light-Curable Resin for Long-term Two-Photon Imaging in Mice. *Bio-Protoc.* **2025**, *15*, e5373. [CrossRef]
58. Xiong, H.; Tang, F.; Guo, Y.; Xu, R.; Lei, P. Neural circuit changes in neurological disorders: Evidence from in vivo two-photon imaging. *Ageing Res. Rev.* **2023**, *87*, 101933. [CrossRef]
59. Greenberg, D.S.; Houweling, A.R.; Kerr, J.N. Population imaging of ongoing neuronal activity in the visual cortex of awake rats. *Nat. Neurosci.* **2008**, *11*, 749–751. [CrossRef]
60. Denk, W.; Svoboda, K. Photon upmanship: Why multiphoton imaging is more than a gimmick. *Neuron* **1997**, *18*, 351–357. [CrossRef]
61. Sabatini, B.L.; Svoboda, K. Analysis of calcium channels in single spines using optical fluctuation analysis. *Nature* **2000**, *408*, 589–593. [CrossRef]
62. Chen, X.; Leischner, U.; Rochefort, N.L.; Nelken, I.; Konnerth, A. Functional mapping of single spines in cortical neurons in vivo. *Nature* **2011**, *475*, 501–505. [CrossRef]
63. Kerr, J.N.; Greenberg, D.; Helmchen, F. Imaging input and output of neocortical networks in vivo. *Proc. Natl. Acad. Sci. USA* **2005**, *102*, 14063–14068. [CrossRef]
64. Ohki, K.; Chung, S.; Ch'ng, Y.H.; Kara, P.; Reid, R.C. Functional imaging with cellular resolution reveals precise micro-architecture in visual cortex. *Nature* **2005**, *433*, 597–603. [CrossRef]
65. Stosiek, C.; Garaschuk, O.; Holthoff, K.; Konnerth, A. In vivo two-photon calcium imaging of neuronal networks. *Proc. Natl. Acad. Sci. USA* **2003**, *100*, 7319–7324. [CrossRef] [PubMed]
66. Kim, T.H.; Zhang, Y.; Lecoq, J.; Jung, J.C.; Li, J.; Zeng, H.; Niell, C.M.; Schnitzer, M.J. Long-Term Optical Access to an Estimated One Million Neurons in the Live Mouse Cortex. *Cell Rep.* **2016**, *17*, 3385–3394. [CrossRef]
67. Cheng, P.; Tian, X.; Tang, W.; Cheng, J.; Bao, J.; Wang, H.; Zheng, S.; Wang, Y.; Wei, X.; Chen, T.; et al. Direct control of store-operated calcium channels by ultrafast laser. *Cell Res.* **2021**, *31*, 758–772. [CrossRef] [PubMed]
68. Tamimi, A.; Caldarola, M.; Hambura, S.; Boffi, J.C.; Noordzij, N.; Los, J.W.N.; Guardiani, A.; Kooiman, H.; Wang, L.; Kieser, C.; et al. Deep Mouse Brain Two-Photon Near-Infrared Fluorescence Imaging Using a Superconducting Nanowire Single-Photon Detector Array. *ACS Photonics* **2024**, *11*, 3960–3971. [CrossRef]
69. Kim, H.M.; Kim, B.R.; An, M.J.; Hong, J.H.; Lee, K.J.; Cho, B.R. Two-photon fluorescent probes for long-term imaging of calcium waves in live tissue. *Chemistry* **2008**, *14*, 2075–2083. [CrossRef]
70. Cao, V.Y.; Ye, Y.; Mastwal, S.S.; Lovinger, D.M.; Costa, R.M.; Wang, K.H. In vivo two-photon imaging of experience-dependent molecular changes in cortical neurons. *J. Vis. Exp.* **2013**, *5*, 50148.
71. Zhao, Z.; Zhou, Y.; Liu, B.; He, J.; Zhao, J.; Cai, Y.; Fan, J.; Li, X.; Wang, Z.; Lu, Z.; et al. Two-photon synthetic aperture microscopy for minimally invasive fast 3D imaging of native subcellular behaviors in deep tissue. *Cell* **2023**, *186*, 2475–2491 e2422. [CrossRef]
72. Zong, W.; Wu, R.; Li, M.; Hu, Y.; Li, Y.; Li, J.; Rong, H.; Wu, H.; Xu, Y.; Lu, Y.; et al. Fast high-resolution miniature two-photon microscopy for brain imaging in freely behaving mice. *Nat. Methods* **2017**, *14*, 713–719. [CrossRef] [PubMed]
73. Zong, W.; Wu, R.; Chen, S.; Wu, J.; Wang, H.; Zhao, Z.; Chen, G.; Tu, R.; Wu, D.; Hu, Y.; et al. Miniature two-photon microscopy for enlarged field-of-view. multi-plane and long-term brain imaging. *Nat. Methods* **2021**, *18*, 46–49. [CrossRef] [PubMed]
74. Wu, R.; Zhao, C.; Qiu, S.; Zhu, Y.; Zhang, L.; Fu, Q.; Hu, Y.; Wu, D.; Yu, F.; Zhou, F.; et al. A versatile miniature two-photon microscope enabling multicolor deep-brain imaging. *Nat. Methods* **2025**, *22*, 1935–1943. [CrossRef]
75. Skoch, J.; Hickey, G.A.; Kajdasz, S.T.; Hyman, B.T.; Bacskai, B.J. In vivo imaging of amyloid-beta deposits in mouse brain with multiphoton microscopy. *Methods Mol. Biol.* **2005**, *299*, 349–363. [PubMed]
76. Bittner, T.; Burgold, S.; Dorostkar, M.M.; Fuhrmann, M.; Wegenast-Braun, B.M.; Schmidt, B.; Kretzschmar, H.; Herms, J. Amyloid plaque formation precedes dendritic spine loss. *Acta Neuropathol.* **2012**, *124*, 797–807. [CrossRef]
77. Meyer-Luehmann, M.; Spires-Jones, T.L.; Prada, C.; Garcia-Alloza, M.; de Calignon, A.; Rozkalne, A.; Koenigsknecht-Talboo, J.; Holtzman, D.M.; Bacskai, B.J.; Hyman, B.T. Rapid appearance and local toxicity of amyloid-beta plaques in a mouse model of Alzheimer's disease. *Nature* **2008**, *451*, 720–724. [CrossRef]

78. Blazquez-Llorca, L.; Valero-Freitag, S.; Rodrigues, E.F.; Merchan-Perez, A.; Rodriguez, J.R.; Dorostkar, M.M.; DeFelipe, J.; Herms, J. High plasticity of axonal pathology in Alzheimer's disease mouse models. *Acta Neuropathol. Commun.* **2017**, *5*, 14. [CrossRef]
79. Busche, M.A.; Wegmann, S.; Dujardin, S.; Commins, C.; Schiantarelli, J.; Klickstein, N.; Kamath, T.V.; Carlson, G.A.; Nelken, I.; Hyman, B.T. Tau impairs neural circuits, dominating amyloid-beta effects, in Alzheimer models in vivo. *Nat. Neurosci.* **2019**, *22*, 57–64. [CrossRef]
80. Zaja-Milatovic, S.; Milatovic, D.; Schantz, A.M.; Zhang, J.; Montine, K.S.; Samii, A.; Deutch, A.Y.; Montine, T.J. Dendritic degeneration in neostriatal medium spiny neurons in Parkinson disease. *Neurology* **2005**, *64*, 545–547. [CrossRef]
81. Maltese, M.; March, J.R.; Bashaw, A.G.; Tritsch, N.X. Dopamine differentially modulates the size of projection neuron ensembles in the intact and dopamine-depleted striatum. *eLife* **2021**, *10*, e68041. [CrossRef]
82. Neuner, J.; Filser, S.; Michalakis, S.; Biel, M.; Herms, J. A30P alpha-Synuclein interferes with the stable integration of adult-born neurons into the olfactory network. *Sci. Rep.* **2014**, *4*, 3931. [CrossRef] [PubMed]
83. Neuner, J.; Ovsepian, S.V.; Dorostkar, M.; Filser, S.; Gupta, A.; Michalakis, S.; Biel, M.; Herms, J. Pathological alpha-synuclein impairs adult-born granule cell development and functional integration in the olfactory bulb. *Nat. Commun.* **2014**, *5*, 3915. [CrossRef]
84. Cahalan, M.D.; Parker, I.; Wei, S.H.; Miller, M.J. Two-photon tissue imaging: Seeing the imune system in a fresh light. *Nat. Rev. Immunol.* **2002**, *2*, 872–880. [CrossRef] [PubMed]
85. Auffray, C.; Fogg, D.; Garfa, M.; Elain, G.; Join-Lambert, O.; Kayal, S.; Sarnacki, S.; Cumano, A.; Lauvau, G.; Geissmann, F. Monitoring of blood vessels and tissues by a population of monocytes with patrolling behavior. *Science* **2007**, *317*, 666–670. [CrossRef]
86. Stamatiades, E.G.; Tremblay, M.E.; Bohm, M.; Crozet, L.; Bisht, K.; Kao, D.; Coelho, C.; Fan, X.; Yewdell, W.T.; Davidson, A.; et al. Immune Monitoring of Trans-endothelial Transport by Kidney-Resident Macrophages. *Cell* **2016**, *166*, 991–1003. [CrossRef]
87. Kim, Y.R.; Kim, Y.M.; Lee, J.; Park, J.; Lee, J.E.; Hyun, Y.M. Neutrophils Return to Bloodstream Through the Brain Blood Vessel After Crosstalk with Microglia During LPS-Induced Neuroinflammation. *Front. Cell Dev. Biol.* **2020**, *8*, 613733. [CrossRef]
88. Park, S.A.; Hyun, Y.M. Neutrophil Extravasation Cascade: What Can We Learn from Two-photon Intravital Imaging? *Immune Netw.* **2016**, *16*, 317–321. [CrossRef]
89. Xu, H.; Lotfy, P.; Gelb, S.; Pragana, A.; Hehnly, C.; Byer, L.I.J.; Shipley, F.B.; Zawadzki, M.E.; Cui, J.; Deng, L.; et al. The choroid plexus synergizes with immune cells during neuroinflammation. *Cell* **2024**, *187*, 4946–4963.e17. [CrossRef]
90. Haage, T.R.; Charakopoulos, E.; Bhuria, V.; Baldauf, C.K.; Korthals, M.; Handschuh, J.; Muller, P.; Li, J.; Harit, K.; Nishanth, G.; et al. Neutrophil-specific expression of JAK2-V617F or CALRmut induces distinct inflammatory profiles in myeloproliferative neoplasia. *J. Hematol. Oncol.* **2024**, *17*, 43. [CrossRef] [PubMed]
91. Kroger, M.; Scheffel, J.; Shirshin, E.A.; Schleusener, J.; Meinke, M.C.; Lademann, J.; Maurer, M.; Darvin, M.E. Label-free imaging of M1 and M2 macrophage phenotypes in the human dermis in vivo using two-photon excited FLIM. *eLife* **2022**, *11*, e72819. [CrossRef] [PubMed]
92. Borowczyk, C.; Laroche-Traineau, J.; Brevier, J.; Jacobin-Valat, M.J.; Marais, S.; Gerbaud, E.; Clofent-Sanchez, G.; Ottones, F. Two-photon excited fluorescence (TPEF) may be useful to identify macrophage subsets based on their metabolic activity and cellular responses in atherosclerotic plaques. *Atherosclerosis* **2020**, *309*, 47–55. [CrossRef]
93. He, B.; Wang, W.; Wen, J.; Zhang, R.; Lin, W.; Guo, Y.; Xu, Y.; Huser, T.; Wei, X.; Yang, Z. Behavioral dynamics of neuroprotective macrophage polarization in neuropathic pain observed by GHz femtosecond laser two-photon excitation microscopy. *J. Biophotonics* **2024**, *17*, e202400026. [CrossRef] [PubMed]
94. Bauer, I.J.; Fang, P.; Lammle, K.F.; Tyystjarvi, S.; Alterauge, D.; Baumjohann, D.; Yoon, H.; Korn, T.; Wekerle, H.; Kawakami, N. Visualizing the activation of encephalitogenic T cells in the ileal lamina propria by in vivo two-photon imaging. *Proc. Natl. Acad. Sci. USA* **2023**, *120*, e2302697120. [CrossRef]
95. MacLean, A.J.; Richmond, N.; Koneva, L.; Attar, M.; Medina, C.A.P.; Thornton, E.E.; Gomes, A.C.; El-Turabi, A.; Bachmann, M.F.; Rijal, P.; et al. Secondary influenza challenge triggers resident memory B cell migration and rapid relocation to boost antibody secretion at infected sites. *Immunity* **2022**, *55*, 718–733 e718. [CrossRef]
96. Cavanagh, L.L.; Weninger, W. Dendritic cell behaviour in vivo: Lessons learned from intravital two-photon microscopy. *Immunol. Cell Biol.* **2008**, *86*, 428–438. [CrossRef]
97. Milo, I.; Blecher-Gonen, R.; Barnett-Itzhaki, Z.; Bar-Ziv, R.; Tal, O.; Gurevich, I.; Feferman, T.; Drexler, I.; Amit, I.; Bousso, P.; et al. The bone marrow is patrolled by NK cells that are primed and expand in response to systemic viral activation. *Eur. J. Immunol.* **2018**, *48*, 1137–1152. [CrossRef] [PubMed]
98. Miller, M.J.; Wei, S.H.; Parker, I.; Cahalan, M.D. Two-photon imaging of lymphocyte motility and antigen response in intact lymph node. *Science* **2002**, *296*, 1869–1873. [CrossRef]
99. Bousso, P.; Bhakta, N.R.; Lewis, R.S.; Robey, E. Dynamics of thymocyte-stromal cell interactions visualized by two-photon microscopy. *Science* **2002**, *296*, 1876–1880. [CrossRef]

100. Celli, S.; Bousso, P. Intravital two-photon imaging of T-cell priming and tolerance in the lymph node. *Methods Mol. Biol.* **2007**, *380*, 355–363.
101. Filipe-Santos, O.; Pescher, P.; Breart, B.; Lippuner, C.; Aebischer, T.; Glaichenhaus, N.; Spath, G.F.; Bousso, P. A dynamic map of antigen recognition by CD4 T cells at the site of Leishmania major infection. *Cell Host Microbe* **2009**, *6*, 23–33. [CrossRef] [PubMed]
102. Loos, J.; Schmaul, S.; Noll, T.M.; Paterka, M.; Schillner, M.; Loffel, J.T.; Zipp, F.; Bittner, S. Functional characteristics of Th1. Th17, and ex-Th17 cells in EAE revealed by intravital two-photon microscopy. *J. Neuroinflamm.* **2020**, *17*, 357. [CrossRef]
103. Tang, Q.; Krummel, M.F. Imaging the function of regulatory T cells in vivo. *Curr. Opin. Immunol.* **2006**, *18*, 496–502. [CrossRef]
104. Guidotti, L.G.; Inverso, D.; Sironi, L.; Di Lucia, P.; Fioravanti, J.; Ganzer, L.; Fiocchi, A.; Vacca, M.; Aiolfi, R.; Sammicheli, S.; et al. Immunosurveillance of the liver by intravascular effector CD8(+) T cells. *Cell* **2015**, *161*, 486–500. [CrossRef]
105. Liu, D.; Yan, J.; Sun, J.; Liu, B.; Ma, W.; Li, Y.; Shao, X.; Qi, H. BCL6 controls contact-dependent help delivery during follicular T-B cell interactions. *Immunity* **2021**, *54*, 2245–2255 e2244. [CrossRef]
106. Stoll, S.; Delon, J.; Brotz, T.M.; Germain, R.N. Dynamic imaging of T cell-dendritic cell interactions in lymph nodes. *Science* **2002**, *296*, 1873–1876. [CrossRef]
107. Mempel, T.R.; Henrickson, S.E.; Von Andrian, U.H. T-cell priming by dendritic cells in lymph nodes occurs in three distinct phases. *Nature* **2004**, *427*, 154–159. [CrossRef]
108. Smokelin, I.; Mizzoni, C.; Erndt-Marino, J.; Kaplan, D.; Georgakoudi, I. Optical changes in THP-1 macrophage metabolism in response to pro- and anti-inflammatory stimuli reported by label-free two-photon imaging. *J. Biomed. Opt.* **2020**, *25*, 014512. [CrossRef] [PubMed]
109. Wang, X.; Wang, X.; Liu, Y.; Sun, Z.; Liu, H.; Shen, J.; Zhu, H.L.; Qian, Y. Activity-Based Imaging of Macrophage Migration Inhibitory Factor with a Two-Photon Fluorescent Probe. *ACS Sens.* **2023**, *8*, 335–343. [CrossRef]
110. Kreiss, L.; Chaware, A.; Roohian, M.; Lemire, S.; Thoma, O.M.; Carle, B.; Waldner, M.; Schurmann, S.; Friedrich, O.; Horstmeyer, R. Cell-MICS: Detecting Immune Cells with Label-Free Two-Photon Autofluorescence and Deep Learning. *J. Biophotonics* **2026**, *19*, e70260. [CrossRef] [PubMed]
111. Gruneboom, A.; Aust, O.; Cibir, Z.; Weber, F.; Hermann, D.M.; Gunzer, M. Imaging innate immunity. *Immunol. Rev.* **2022**, *306*, 293–303. [CrossRef] [PubMed]
112. Liew, P.X.; Kubes, P. The Neutrophil's Role During Health and Disease. *Physiol. Rev.* **2019**, *99*, 1223–1248. [CrossRef]
113. Palomino-Segura, M.; Gonzalez, S.F. Two-Photon Intravital Imaging of Leukocytes in the Trachea During Pneumococcal Infection. *Methods Mol. Biol.* **2019**, *1968*, 183–194. [PubMed]
114. Lammermann, T.; Afonso, P.V.; Angermann, B.R.; Wang, J.M.; Kastenmuller, W.; Parent, C.A.; Germain, R.N. Neutrophil swarms require LTB4 and integrins at sites of cell death in vivo. *Nature* **2013**, *498*, 371–375. [CrossRef]
115. Kohler, A.; De Filippo, K.; Hasenberg, M.; van den Brandt, C.; Nye, E.; Hosking, M.P.; Lane, T.E.; Mann, L.; Ransohoff, R.M.; Hauser, A.E.; et al. G-CSF-mediated thrombopoietin release triggers neutrophil motility and mobilization from bone marrow via induction of Cxcr2 ligands. *Blood* **2011**, *117*, 4349–4357. [CrossRef]
116. Neumann, J.; Riek-Burchardt, M.; Herz, J.; Doeppner, T.R.; Konig, R.; Hutten, H.; Etemire, E.; Mann, L.; Klingberg, A.; Fischer, T.; et al. Very-late-antigen-4 (VLA-4)-mediated brain invasion by neutrophils leads to interactions with microglia. increased ischemic injury and impaired behavior in experimental stroke. *Acta Neuropathol.* **2015**, *129*, 259–277. [CrossRef]
117. Freeman, S.A.; Uderhardt, S.; Saric, A.; Collins, R.F.; Buckley, C.M.; Mylvaganam, S.; Boroumand, P.; Plumb, J.; Germain, R.N.; Ren, D.; et al. Lipid-gated monovalent ion fluxes regulate endocytic traffic and support immune surveillance. *Science* **2020**, *367*, 301–305. [CrossRef]
118. Wang, J.; Kubes, P. A Reservoir of Mature Cavity Macrophages that Can Rapidly Invade Visceral Organs to Affect Tissue Repair. *Cell* **2016**, *165*, 668–678. [CrossRef]
119. Gao, X.; Huang, X.; Chen, Z.; Yang, L.; Zhou, Y.; Hou, Z.; Yang, J.; Qi, S.; Liu, Z.; Zhang, Z.; et al. Supercontinuum-tailoring multicolor imaging reveals spatiotemporal dynamics of heterogeneous tumor evolution. *Nat. Commun.* **2024**, *15*, 9313. [CrossRef] [PubMed]
120. Bousso, P. Diving into the mechanism of action of tumor immunotherapies with intravital imaging. *Immunol. Rev.* **2022**, *306*, 218–223. [CrossRef]
121. Kolesnikov, M.; Farache, J.; Shakhar, G. Intravital two-photon imaging of the gastrointestinal tract. *J. Immunol. Methods* **2015**, *421*, 73–80. [CrossRef]
122. Ma, B.; Liu, F.; Zhang, S.; Duan, J.; Kong, Y.; Li, Z.; Tang, D.; Wang, W.; Ge, S.; Tang, W.; et al. Two-photon fluorescent polydopamine nanodots for CAR-T cell function verification and tumor cell/tissue detection. *J. Mater. Chem. B* **2018**, *6*, 6459–6467. [CrossRef] [PubMed]
123. Arlauckas, S.P.; Garris, C.S.; Kohler, R.H.; Kitaoka, M.; Cuccarese, M.F.; Yang, K.S.; Miller, M.A.; Carlson, J.C.; Freeman, G.J.; Anthony, R.M.; et al. In vivo imaging reveals a tumor-associated macrophage-mediated resistance pathway in anti-PD-1 therapy. *Sci. Transl. Med.* **2017**, *9*, eaal3604. [CrossRef]

124. Wang, L.; Karges, J.; Wei, F.; Xie, L.; Chen, Z.; Gasser, G.; Ji, L.; Chao, H. A mitochondria-localized iridium(III) photosensitizer for two-photon photodynamic immunotherapy against melanoma. *Chem. Sci.* **2023**, *14*, 1461–1471. [CrossRef] [PubMed]
125. Tan, Y.; Hu, G.; Li, M.; An, Y.; Wang, Z.; Liu, R.; Xu, D.; Tan, X.; Zeng, Y.; He, Y.; et al. Two-photon photosensitizer for specific targeting and induction of tumor pyroptosis to elicit systemic immunity-boosting anti-tumor therapy. *Biomaterials* **2025**, *317*, 123108. [CrossRef]
126. Perry, S.W.; Burke, R.M.; Brown, E.B. Two-photon and second harmonic microscopy in clinical and translational cancer research. *Ann. Biomed. Eng.* **2012**, *40*, 277–291. [CrossRef]
127. Rogart, J.N.; Nagata, J.; Loeser, C.S.; Roorda, R.D.; Aslanian, H.; Robert, M.E.; Zipfel, W.R.; Nathanson, M.H. Multiphoton imaging can be used for microscopic examination of intact human gastrointestinal mucosa ex vivo. *Clin. Gastroenterol. Hepatol.* **2008**, *6*, 95–101. [CrossRef]
128. Williams, R.M.; Flesken-Nikitin, A.; Ellenson, L.H.; Connolly, D.C.; Hamilton, T.C.; Nikitin, A.Y.; Zipfel, W.R. Strategies for high resolution imaging of epithelial ovarian cancer by laparoscopic nonlinear microscopy. *Transl. Oncol.* **2010**, *3*, 181–194. [CrossRef]
129. Huang, Z.; Li, Z.; Chen, R.; Lin, J.; Li, Y.; Li, C. In vitro imaging of thyroid tissues using two-photon excited fluorescence and second harmonic generation. *Photomed. Laser Surg.* **2010**, *28*, S129–S133. [CrossRef] [PubMed]
130. Gatesman Ammer, A.; Hayes, K.E.; Martin, K.H.; Zhang, L.; Spirou, G.A.; Weed, S.A. Multi-photon imaging of tumor cell invasion in an orthotopic mouse model of oral squamous cell carcinoma. *J. Vis. Exp.* **2011**, *25*, 2941.
131. Yan, J.; Chen, G.; Chen, J.; Liu, N.; Zhuo, S.; Yu, H.; Ying, M. A pilot study of using multiphoton microscopy to diagnose gastric cancer. *Surg. Endosc.* **2011**, *25*, 1425–1430. [CrossRef]
132. Tewari, A.K.; Shevchuk, M.M.; Sterling, J.; Grover, S.; Herman, M.; Yadav, R.; Mudalair, K.; Srivastava, A.; Rubin, M.A.; Zipfel, W.R. Multiphoton microscopy for structure identification in human prostate and periprostatic tissue: Implications in prostate cancer surgery. *BJU Int.* **2011**, *108*, 1421–1429. [CrossRef] [PubMed]
133. Li, L.; Huang, X.; Zhang, S.; Zhan, Z.; Kang, D.; Guan, G.; Xu, S.; Zhou, Y.; Chen, J. Rapid and label-free detection of gastrointestinal stromal tumor via a combination of two-photon microscopy and imaging analysis. *BMC Cancer* **2023**, *23*, 38. [CrossRef] [PubMed]
134. Li, L.; Hong, S.; Kang, D.; Huang, X.; Zhang, S.; Zhang, Z.; Zhou, Y.; Chen, J. Two-photon imaging reveals histopathological changes in the gastric tumor microenvironment induced by neoadjuvant treatment. *Biomed. Opt. Express* **2023**, *14*, 5085–5096. [CrossRef] [PubMed]
135. Wang, B.G.; Konig, K.; Halbhuber, K.J. Two-photon microscopy of deep intravital tissues and its merits in clinical research. *J. Microsc.* **2010**, *238*, 1–20. [CrossRef]
136. Kong, X.; Dong, B.; Zhang, N.; Wang, C.; Song, X.; Lin, W. A unique red-emitting two-photon fluorescent probe with tumor-specificity for imaging in living cells and tissues. *Talanta* **2017**, *174*, 357–364. [CrossRef]
137. Liu, Y.; Liu, W.; Li, H.; Yan, W.; Yang, X.; Liu, D.; Wang, S.; Zhang, J. Two-photon fluorescent probe for detection of nitroreductase and hypoxia-specific microenvironment of cancer stem cell. *Anal. Chim. Acta* **2018**, *1024*, 177–186. [CrossRef]
138. Zha, Y.; Cui, X.; Liu, Y.; Fan, S.; Lu, Y.; Cui, S.; Cui, D. Two-Photon Nanoprobe for NIR-II Imaging of Tumour and Biosafety Evaluation. *J. Biomed. Nanotechnol.* **2022**, *18*, 807–817. [CrossRef]
139. Jiang, W.; An, W.; Huang, Z.; Xu, C.; Shen, Q.; Pu, C.; Zhang, S.; Wu, Q.; Li, L.; Yu, C. A near-infrared fluorescent probe with two-photon excitation for in situ imaging of NQO1 in human colorectum cancer tissue. *Talanta* **2024**, *274*, 126018. [CrossRef]
140. Hao, L.; Ni, Y.; Huang, J.; Wang, Y.; Liu, F.; Wang, X.; Kang, L.; Lin, Z.; Zhu, W. Near-Infrared Cocrystal Nanofluorophore with Enhanced Two-Photon Absorption Cross Sections. *Adv. Sci.* **2026**, *13*, e23319. [CrossRef]
141. Warburg, O.; Wind, F.; Negelein, E. The Metabolism of Tumors in the Body. *J. Gen. Physiol.* **1927**, *8*, 519–530. [CrossRef] [PubMed]
142. Xu, H.N.; Tchou, J.; Feng, M.; Zhao, H.; Li, L.Z. Optical redox imaging indices discriminate human breast cancer from normal tissues. *J. Biomed. Opt.* **2016**, *21*, 114003. [CrossRef]
143. Bird, D.K.; Yan, L.; Vrotsos, K.M.; Eliceiri, K.W.; Vaughan, E.M.; Keely, P.J.; White, J.G.; Ramanujam, N. Metabolic mapping of MCF10A human breast cells via multiphoton fluorescence lifetime imaging of the coenzyme NADH. *Cancer Res.* **2005**, *65*, 8766–8773. [CrossRef]
144. Yu, Q.; Heikal, A.A. Two-photon autofluorescence dynamics imaging reveals sensitivity of intracellular NADH concentration and conformation to cell physiology at the single-cell level. *J. Photochem. Photobiol. B* **2009**, *95*, 46–57. [CrossRef] [PubMed]
145. Shah, A.T.; Demory Beckler, M.; Walsh, A.J.; Jones, W.P.; Pohlmann, P.R.; Skala, M.C. Optical metabolic imaging of treatment response in human head and neck squamous cell carcinoma. *PLoS ONE* **2014**, *9*, e90746. [CrossRef]
146. Cong, A.; Pimenta, R.M.L.; Lee, H.B.; Mereddy, V.; Holy, J.; Heikal, A.A. Two-photon fluorescence lifetime imaging of intrinsic NADH in three-dimensional tumor models. *Cytom. A* **2019**, *95*, 80–92. [CrossRef] [PubMed]
147. Zhang, J.; Wallrabe, H.; Siller, K.; Mbogo, B.; Cassidy, T.; Alam, S.R.; Periasamy, A. Measuring Metabolic Changes in Cancer Cells Using Two-Photon Fluorescence Lifetime Imaging Microscopy and Machine-Learning Analysis. *J. Biophotonics* **2025**, *18*, e202400426. [CrossRef]
148. Liang, W.; Chen, D.; Guan, H.; Park, H.-C.; Li, K.; Li, A.; Li, M.-J.; Gannot, I.; Li, X. Label-free metabolic imaging in vivo by two-photon fluorescence lifetime endomicroscopy. *ACS Photonics* **2022**, *9*, 4017–4029. [CrossRef]

149. Zou, Y.; Li, M.; Xing, Y.; Duan, T.; Zhou, X.; Yu, F. Bioimaging of glutathione with a two-photon fluorescent probe and its potential application for surgery guide in laryngeal cancer. *ACS Sens.* **2019**, *5*, 242–249. [CrossRef]
150. Wang, W.; Wang, C.; Liu, G.; Jin, L.; Lin, Z.; Lin, L.; Wu, Y.; Chen, J.; Lin, H.; Song, J. In-vivo two-photon visualization and quantitative detection of redox state of cancer. *J. Biophotonics* **2022**, *15*, e202100357. [CrossRef] [PubMed]
151. Mao, G.-J.; Zhang, S.-Y.; Yang, T.-T.; Zhu, B.; Sun, X.-Y.; Wang, Q.-Q.; Zhang, G. A tumor-targeting two-photon fluorescent probe with a far-red to NIR emission for imaging basal hypochlorite in cancer cells and tumor. *Talanta* **2024**, *277*, 126436. [CrossRef]
152. Luo, X.; Yu, F.; Wang, R.; Su, T.; Luo, P.; Wen, P.; Yu, F. A near-infrared two-photon fluorescent probe for the detection of HClO in inflammatory and tumor-bearing mice. *Chin. Chem. Lett.* **2025**, *36*, 110531. [CrossRef]
153. Zhai, B.; Hu, W.; Zhai, S.; Liang, T.; Liu, Z. Two-photon imaging for visualizing polarity in lipid droplets during chemotherapy induced Ferroptosis. *Talanta* **2023**, *256*, 124304. [CrossRef] [PubMed]
154. Wu, T.; Liao, J.; Xiang, F.; Yu, J.; Huo, Y.; Gao, Y.; Li, H.; Zheng, W. Probing cell metabolism using the two-photon excitation autofluorescence lifetime of tryptophan. *Opt. Lett.* **2024**, *49*, 1105–1108. [CrossRef] [PubMed]
155. Tozer, G.M.; Ameer-Beg, S.M.; Baker, J.; Barber, P.R.; Hill, S.A.; Hodgkiss, R.J.; Locke, R.; Prise, V.E.; Wilson, I.; Vojnovic, B. Intravital imaging of tumour vascular networks using multi-photon fluorescence microscopy. *Adv. Drug Deliv. Rev.* **2005**, *57*, 135–152. [CrossRef]
156. Fukumura, D.; Duda, D.G.; Munn, L.L.; Jain, R.K. Tumor microvasculature and microenvironment: Novel insights through intravital imaging in pre-clinical models. *Microcirculation* **2010**, *17*, 206–225. [CrossRef]
157. Morales, A.R.; Yanez, C.O.; Zhang, Y.; Wang, X.; Biswas, S.; Urakami, T.; Komatsu, M.; Belfield, K.D. Small molecule fluorophore and copolymer RGD peptide conjugates for ex vivo two-photon fluorescence tumor vasculature imaging. *Biomaterials* **2012**, *33*, 8477–8485. [CrossRef]
158. Yue, X.; Morales, A.R.; Githaiga, G.W.; Woodward, A.W.; Tang, S.; Sawada, J.; Komatsu, M.; Liu, X.; Belfield, K.D. RGD-conjugated two-photon absorbing near-IR emitting fluorescent probes for tumor vasculature imaging. *Org. Biomol. Chem.* **2015**, *13*, 10716–10725. [CrossRef]
159. Wang, S.; Liu, J.; Goh, C.C.; Ng, L.G.; Liu, B. NIR-II-excited intravital two-photon microscopy distinguishes deep cerebral and tumor vasculatures with an ultrabright NIR-I AIE luminogen. *Adv. Mater.* **2019**, *31*, 1904447. [CrossRef]
160. Enache, A.; Eftimie, L.; Graur, A.; Glogojeanu, R.; Geambasu, A.; Voinea, O. Assessment of cerebral tumors and metastases by two-photon excitation microscopy. *Rom. J. Mil. Med.* **2023**, *126*, 418–423. [CrossRef]
161. Ilina, O.; Bakker, G.-J.; Vasaturo, A.; Hoffman, R.M.; Friedl, P. Two-photon laser-generated microtracks in 3D collagen lattices: Principles of MMP-dependent and-independent collective cancer cell invasion. *Phys. Biol.* **2011**, *8*, 015010. [CrossRef] [PubMed]
162. Zhang, W.; Karschnia, P.; von Mücke-Heim, I.-A.; Mulazzani, M.; Zhou, X.; Blobner, J.; Mueller, N.; Teske, N.; Dede, S.; Xu, T. In vivo two-photon characterization of tumor-associated macrophages and microglia (TAM/M) and CX3CR1 during different steps of brain metastasis formation from lung cancer. *Neoplasia* **2021**, *23*, 1089–1100.
163. Xu, T.; Karschnia, P.; Cadilha, B.L.; Dede, S.; Lorenz, M.; Seewaldt, N.; Nikolaishvili, E.; Müller, K.; Blobner, J.; Teske, N. In vivo dynamics and anti-tumor effects of EpCAM-directed CAR T-cells against brain metastases from lung cancer. *Oncoimmunology* **2023**, *12*, 2163781. [CrossRef] [PubMed]
164. Xu, C.; Law, S.K.; Leung, A.W.N. Comparison of the Differences between Two-Photon Excitation. Upconversion, and Conventional Photodynamic Therapy on Cancers in In Vitro and In Vivo Studies. *Pharmaceuticals* **2024**, *17*, 663. [CrossRef]
165. Bhawalkar, J.; Kumar, N.; Zhao, C.-F.; Prasad, P.N. Two-photon photodynamic therapy. *J. Clin. Laser Med. Surg.* **1997**, *15*, 201–204. [CrossRef]
166. Luo, T.; Wilson, B.C.; Lu, Q.-B. Evaluation of one-and two-photon activated photodynamic therapy with pyropheophorbide-a methyl ester in human cervical. lung and ovarian cancer cells. *J. Photochem. Photobiol. B* **2014**, *132*, 102–110. [CrossRef] [PubMed]
167. McKenzie, L.K.; Sazanovich, I.V.; Baggaley, E.; Bonneau, M.; Guerchais, V.; Williams, J.A.; Weinstein, J.A.; Bryant, H.E. Metal Complexes for Two-Photon Photodynamic Therapy: A Cyclometallated Iridium Complex Induces Two-Photon Photosensitization of Cancer Cells under Near-IR Light. *Chemistry* **2017**, *23*, 234–238.
168. Wang, S.; Wang, J.; Chen, J.Y. Conjugates of folic acids with zinc aminophthalocyanine for cancer cell targeting and photodynamic therapy by one-photon and two-photon excitations. *J. Mater. Chem. B* **2014**, *2*, 1594–1602. [CrossRef]
169. Ogawa, K.; Kobuke, Y. Two-Photon Photodynamic Therapy by Water-Soluble Self-Assembled Conjugated Porphyrins. *BioMed Res. Int.* **2013**, *2013*, 125658. [CrossRef]
170. Chennoufi, R.; Mahuteau-Betzer, F.; Tauc, P.; Teulade-Fichou, M.P.; Deprez, E. Triphenylamines Induce Cell Death Upon 2-Photon Excitation. *Mol. Imaging* **2017**, *16*, 1536012117714164. [CrossRef]
171. Zhou, J.; Ji, M.; Yang, Y.; Su, W.; Chen, L.; Liu, Y.; Fei, Y.; Ma, J.; Mi, L. Two-photon photodynamic therapy with curcumin nanocomposite. *Colloids Surf. B Biointerfaces* **2025**, *245*, 114306. [CrossRef]
172. Zhao, Z.; Qiu, K.; Liu, J.; Hao, X.; Wang, J. Two-photon photodynamic ablation of tumour cells using an RGD peptide-conjugated ruthenium (ii) photosensitiser. *Chem. Commun.* **2020**, *56*, 12542–12545. [CrossRef] [PubMed]

173. Kuang, S.; Sun, L.; Zhang, X.; Liao, X.; Rees, T.W.; Zeng, L.; Chen, Y.; Zhang, X.; Ji, L.; Chao, H. A mitochondrion-localized two-photon photosensitizer generating carbon radicals against hypoxic tumors. *Angew. Chem. Int. Ed. Engl.* **2020**, *59*, 20697–20703. [CrossRef] [PubMed]
174. Rice, W.L.; Kaplan, D.L.; Georgakoudi, I. Two-photon microscopy for non-invasive. quantitative monitoring of stem cell differentiation. *PLoS ONE* **2010**, *5*, e10075. [CrossRef] [PubMed]
175. Meleshina, A.V.; Dudenkova, V.V.; Shirmanova, M.V.; Shcheslavskiy, V.I.; Becker, W.; Bystrova, A.S.; Cherkasova, E.I.; Zagaynova, E.V. Probing metabolic states of differentiating stem cells using two-photon FLIM. *Sci. Rep.* **2016**, *6*, 21853. [CrossRef]
176. Meleshina, A.V.; Dudenkova, V.V.; Bystrova, A.S.; Kuznetsova, D.S.; Shirmanova, M.V.; Zagaynova, E.V. Two-photon FLIM of NAD(P)H and FAD in mesenchymal stem cells undergoing either osteogenic or chondrogenic differentiation. *Stem Cell Res. Ther.* **2017**, *8*, 15. [CrossRef]
177. Huang, S.; Rompolas, P. Two-photon microscopy for intracutaneous imaging of stem cell activity in mice. *Exp. Dermatol.* **2017**, *26*, 379–383. [CrossRef]
178. Farrelly, O.; Suzuki-Horiuchi, Y.; Brewster, M.; Kuri, P.; Huang, S.; Rice, G.; Bae, H.; Xu, J.; Dentchev, T.; Lee, V.; et al. Two-photon live imaging of single corneal stem cells reveals compartmentalized organization of the limbal niche. *Cell Stem Cell* **2021**, *28*, 1233–1247.e4. [CrossRef]
179. Sudo, T.; Yamashita, E.; Kikuta, J.; Ishii, M. Protocol for live imaging of transferred mouse bone marrow cells by two-photon microscopy. *STAR Protoc.* **2023**, *4*, 102654. [CrossRef]
180. Ma, N.; Mourkioti, F. Ex vivo two-photon imaging of whole-mount skeletal muscles to visualize stem cell behavior. *STAR Protoc.* **2024**, *5*, 102772. [CrossRef]
181. Wang, Q.; Jin, Y.; Deng, X.; Liu, H.; Pang, H.; Shi, P.; Zhan, Z. Second-harmonic generation microscopy for assessment of mesenchymal stem cell-seeded acellular dermal matrix in wound-healing. *Biomaterials* **2015**, *53*, 659–668. [CrossRef]
182. Wallenburg, M.A.; Wu, J.; Li, R.K.; Vitkin, I.A. Two-photon microscopy of healthy. infarcted and stem-cell treated regenerating heart. *J. Biophotonics* **2011**, *4*, 297–304. [PubMed]
183. Zhang, K.; Chen, S.; Sun, H.; Wang, L.; Li, H.; Zhao, J.; Zhang, C.; Li, N.; Guo, Z.; Han, Z.; et al. In vivo two-photon microscopy reveals the contribution of Sox9(+) cell to kidney regeneration in a mouse model with extracellular vesicle treatment. *J. Biol. Chem.* **2020**, *295*, 12203–12213. [CrossRef] [PubMed]
184. Shen, B.; Wei, H.; Wen, Y.; Geng, Y.; Yang, T.; Chen, Z.; Dong, S.; Gao, Y.; Li, T.; Sun, L.; et al. Optimized in vivo two-photon imaging reveals the essential role of the contralateral eye in functional optic nerve regeneration in zebrafish larvae. *Eye Vis.* **2025**, *12*, 34. [CrossRef] [PubMed]
185. Villasenor, S.; Grinstein, M. Two-Photon Microscopy for the Study of Tendons. *J. Vis. Exp.* **2024**, *205*, e65853.
186. Kamiya, T.; Ito, Y.; Iwasaki, T.; Suzuki, D.; Hayashi, T.; Kim, J.; Matsumoto, T.; Maeda, E. Structural characterization of newt tendon regeneration after complete transection: In vivo two-photon imaging and transmission electron microscopy. *J. Anat.* **2026**, *248*, 383–394.
187. Agemura, T.; Hasegawa, T.; Yari, S.; Kikuta, J.; Ishii, M. Arthritis-associated osteoclastogenic macrophage. AtoM, as a key player in pathological bone erosion. *Inflamm. Regen.* **2022**, *42*, 17. [CrossRef]
188. Lee, M.; Kannan, S.; Muniraj, G.; Rosa, V.; Lu, W.F.; Fuh, J.Y.; Sriram, G.; Cao, T. Two-photon fluorescence microscopy and applications in angiogenesis and related molecular events. *Tissue Eng. Part B Rev.* **2022**, *28*, 926–937. [CrossRef]
189. Keshara, R.; Kim, Y.H.; Grapin-Botton, A. Organoid imaging: Seeing development and function. *Annu. Rev. Cell Dev. Biol.* **2022**, *38*, 447–466. [CrossRef]
190. Tomasi, S.; Scuderi, S.; Amiri, A.; Altobelli, G.G.; Mariani, J.; Dambrot, C.; Coppola, G.; Vaccarino, F.M. High-resolution molecular phenotyping of human IPSC organoids using CLARITY and 2-photon microscopy. In *Neuroscience*; IRIS: San Diego, CA, USA, 2016.
191. Wilson, M.N.; Thunemann, M.; Liu, X.; Lu, Y.; Puppo, F.; Adams, J.W.; Kim, J.-H.; Ramezani, M.; Pizzo, D.P.; Djurovic, S. Multimodal monitoring of human cortical organoids implanted in mice reveal functional connection with visual cortex. *Nat. Commun.* **2022**, *13*, 7945. [CrossRef]
192. Xue, Y.; Browne, A.W.; Tang, W.C.; Delgado, J.; McLelland, B.T.; Nistor, G.; Chen, J.T.; Chew, K.; Lee, N.; Keirstead, H.S. Retinal organoids long-term functional characterization using two-photon fluorescence lifetime and hyperspectral microscopy. *Front. Cell. Neurosci.* **2021**, *15*, 796903. [CrossRef]
193. Khoshravesh, R.; Hoffmann, N.; Hanson, D.T. Leaf microscopy applications in photosynthesis research: Identifying the gaps. *J. Exp. Bot.* **2022**, *73*, 1868–1893. [CrossRef]
194. Su, C.; Liu, Z.; Sun, X.; Zhang, R.; Sun, Q.; Wu, M.; Niu, N.; Chen, L. Development and application of two-photon fluorescent probe for visual monitoring of isoprene in plants. *J. Hazard. Mater.* **2025**, *500*, 140378. [CrossRef]
195. Tai, S.P.; Chan, M.C.; Tsai, T.H.; Guol, S.H.; Chen, L.J.; Sun, C.K. Two-photon fluorescence microscope with a hollow-core photonic crystal fiber. *Opt. Express* **2004**, *12*, 6122–6128. [CrossRef] [PubMed]

196. Mizuta, Y.; Kurihara, D.; Higashiyama, T. Two-photon imaging with longer wavelength excitation in intact Arabidopsis tissues. *Protoplasma* **2015**, *252*, 1231–1240. [CrossRef] [PubMed]
197. Iermak, I.; Vink, J.; Bader, A.N.; Wientjes, E.; van Amerongen, H. Visualizing heterogeneity of photosynthetic properties of plant leaves with two-photon fluorescence lifetime imaging microscopy. *Biochim. Biophys. Acta* **2016**, *1857*, 1473–1478. [CrossRef]
198. Zhang, N.; Chang, H.; Miao, R.; Liu, T.; Ding, L.; Fang, Y. Structure-activity relationships of aniline-based squaraines for distinguishable staining and bright two-photon fluorescence bioimaging in plant cells. *J. Mater. Chem. B* **2024**, *12*, 5350–5359. [CrossRef]
199. Rosa, S.; Shaw, P. Two-photon Photoactivation to Measure Histone Exchange Dynamics in Plant Root Cells. *Bio-Protoc.* **2015**, *5*, e1628.
200. Wang, P.F.; Lin, D.Y.; Ma, W.Y. Observation on cytoskeleton and root tip growth of Arabidopsis thaliana by two-photon laser scanning microscopy. *Spectrosc. Spectr. Anal.* **2010**, *30*, 2593–2596.
201. Murata, T.; Tsutsumi, M.; Otomo, K.; Nemoto, T. Cell Division Imaging of Tobacco BY-2 Cells in a 3D Volume by Two-Photon Spinning-Disk Confocal Microscopy. *Methods Mol. Biol.* **2025**, *2872*, 37–50. [PubMed]
202. Safaee, M.M.; McFarlane, I.R.; Nishitani, S.; Yang, S.J.; Sun, E.; Medina, S.M.; Squire, H.; Landry, M.P. Dual Infrared 2-Photon Microscopy Achieves Minimal Background Deep Tissue Imaging in Brain and Plant Tissues. *Adv. Funct. Mater.* **2024**, *34*, 2404709. [CrossRef]
203. Chen, Z.; Li, J.; Wang, B.C.; Tian, L. In vivo two-photon FLIM resolves photosynthetic properties of maize bundle sheath cells. *Photosynth. Res.* **2025**, *163*, 11. [CrossRef]
204. Stoneman, M.R.; McCoy, V.E.; Gee, C.T.; Bober, K.M.M.; Raicu, V. Two-photon excitation fluorescence microspectroscopy protocols for examining fluorophores in fossil plants. *Commun. Biol.* **2024**, *7*, 53. [CrossRef]
205. Ryu, J.; Nam, H.; Kim, H.K.; Joo, Y.; Lee, S.J.; Kim, K.H. In vivo monitoring of intracellular chloroplast movements in intact leaves of C4 plants using two-photon microscopy. *Microsc. Res. Tech.* **2014**, *77*, 806–813. [CrossRef] [PubMed]
206. Liao, J.N.; Chen, W.L.; Lo, C.Y.; Lai, M.H.; Tsai, H.L.; Chang, Y.M. Nondestructive circadian profiling of starch content in fresh intact Arabidopsis leaf with two-photon fluorescence and second-harmonic generation imaging. *Sci. Rep.* **2022**, *12*, 16525. [CrossRef]
207. Zeng, Y.; Wu, Y.; Li, D.; Zheng, W.; Wang, W.X.; Qu, J.Y. Two-photon excitation chlorophyll fluorescence lifetime imaging: A rapid and noninvasive method for in vivo assessment of cadmium toxicity in a marine diatom *Thalassiosira weissflogii*. *Planta* **2012**, *236*, 1653–1663. [CrossRef]
208. Asghar, S.; Yu, Z.; Zhu, Z.; Zheng, D.; Zhao, Z.; Xu, Y.; Liu, X.; Yuan, C.; Li, Y.; Wang, W.; et al. Visualization of Hg(2+) Stress on Plant Health at the Subcellular Level Revealed by a Highly Sensitive Fluorescent Sensor. *Research* **2025**, *8*, 0570. [CrossRef]
209. Mizuta, Y. Advances in Two-Photon Imaging in Plants. *Plant Cell Physiol.* **2021**, *62*, 1224–1230. [CrossRef] [PubMed]
210. Oh, S.W.; Harris, J.A.; Ng, L.; Winslow, B.; Cain, N.; Mihalas, S.; Wang, Q.; Lau, C.; Kuan, L.; Henry, A.M.; et al. A mesoscale connectome of the mouse brain. *Nature* **2014**, *508*, 207–214. [CrossRef] [PubMed]
211. Kulkarni, R.U.; Vandenberghe, M.; Thunemann, M.; James, F.; Andreassen, O.A.; Djurovic, S.; Devor, A.; Miller, E.W. In Vivo Two-Photon Voltage Imaging with Sulfonated Rhodamine Dyes. *ACS Cent. Sci.* **2018**, *4*, 1371–1378. [CrossRef]
212. Yang, M.; Zhou, Z.; Zhang, J.; Jia, S.; Li, T.; Guan, J.; Liao, X.; Leng, B.; Lyu, J.; Zhang, K.; et al. MATRIEX imaging: Multiarea two-photon real-time in vivo explorer. *Light Sci. Appl.* **2019**, *8*, 109. [PubMed]
213. Lu, Q.; Wu, C.J.; Liu, Z.; Niu, G.; Yu, X. Fluorescent AIE-Active Materials for Two-Photon Bioimaging Applications. *Front. Chem.* **2020**, *8*, 617463. [CrossRef]
214. Tu, Y.X.; Vijay, N.; Ko, H.X.; Lo, Y.P.; Velmathi, S.; Wu, S.P. Specific two-photon fluorescent probe for cysteine detection in vivo. *Spectrochim. Acta A Mol. Biomol. Spectrosc.* **2022**, *267*, 120521. [CrossRef]
215. Wang, M.; Chen, J.; Wu, W.; Wang, L.; Zheng, X.; Xu, G.; Qu, J.; Gao, B.Z.; Shao, Y. Multi-color two-photon scanning structured illumination microscopy imaging of live cells. *J. Biophotonics* **2023**, *16*, e202300077. [CrossRef] [PubMed]
216. Moneron, G.; Hell, S.W. Two-photon excitation STED microscopy. *Opt. Express* **2009**, *17*, 14567–14573. [CrossRef]
217. Iyer, V.; Hoogland, T.M.; Saggau, P. Fast functional imaging of single neurons using random-access multiphoton (RAMP) microscopy. *J. Neurophysiol.* **2006**, *95*, 535–545. [CrossRef]
218. Nadella, K.M.; Ros, H.; Baragli, C.; Griffiths, V.A.; Konstantinou, G.; Koimtzis, T.; Evans, G.J.; Kirkby, P.A.; Silver, R.A. Random-access scanning microscopy for 3D imaging in awake behaving animals. *Nat. Methods* **2016**, *13*, 1001–1004. [CrossRef]
219. Pisanello, M.; Zheng, D.; Balena, A.; Pisano, F.; De Vittorio, M.; Pisanello, F. An open source three-mirror laser scanning holographic two-photon lithography system. *PLoS ONE* **2022**, *17*, e0265678.
220. Srivastava, P.; Stierwalt, D.A.; Elles, C.G. Broadband Two-Photon Absorption Spectroscopy with Stimulated Raman Scattering as an Internal Standard. *Anal. Chem.* **2023**, *95*, 13227–13234. [CrossRef]
221. Wang, D.; Wei, W.; Singh, A.; He, G.S.; Kannan, R.; Tan, L.S.; Chen, G.; Prasad, P.N.; Xia, J. Nonlinear Photoacoustic Imaging by in situ Multiphoton Upconversion and Energy Transfer. *ACS Photonics* **2017**, *4*, 2699–2705. [CrossRef] [PubMed]

222. Ranawat, H.; Pal, S.; Mazumder, N. Recent trends in two-photon auto-fluorescence lifetime imaging (2P-FLIM) and its biomedical applications. *Biomed. Eng. Lett.* **2019**, *9*, 293–310. [CrossRef] [PubMed]
223. Adesnik, H.; Abdeladim, L. Probing neural codes with two-photon holographic optogenetics. *Nat. Neurosci.* **2021**, *24*, 1356–1366. [CrossRef] [PubMed]
224. Liu, D.; Sun, X.M.; Zhu, L.; Li, C.Y. Using time-shared scanning optical tweezers assisted two-photon fluorescence imaging to establish a versatile CRISPR/Cas12a-mediated biosensor. *Biosens. Bioelectron.* **2023**, *227*, 115158. [CrossRef] [PubMed]

Disclaimer/Publisher's Note: The statements, opinions and data contained in all publications are solely those of the individual author(s) and contributor(s) and not of MDPI and/or the editor(s). MDPI and/or the editor(s) disclaim responsibility for any injury to people or property resulting from any ideas, methods, instructions or products referred to in the content.